Study of light-meson resonances decaying to $K^0_\mathrm{S} K\pi$ in the $B \to (K^0_\mathrm{S} K\pi)K$ channels

R. Aaij *et al.*[*]
(LHCb Collaboration)

(Received 14 January 2025; accepted 15 April 2025; published 15 May 2025)

A study is presented of $B^+ \to K^0_\mathrm{S} K^- \pi^+ K^+$ and $B^+ \to K^0_\mathrm{S} K^+ \pi^- K^+$ decays based on the analysis of proton-proton collision data collected with the LHCb detector at center-of-mass energies of 7, 8 and 13 TeV, corresponding to an integrated luminosity of 9 fb^{-1}. The $K^0_\mathrm{S} K\pi$ invariant-mass distributions of both B^+ decay modes show, in the $m(K^0_\mathrm{S} K\pi) < 1.85$ GeV mass region, large activity which is resolved using an amplitude analysis. A simple model, where J^{PC} amplitudes are described by multiple Breit-Wigner functions with appropriate angular distributions, provides a good description of the experimental data. In this approach a complex mixture of $J^{PC} = 0^{-+}$, 1^{++} and 1^{+-} amplitudes is observed that is dominated by $\eta(1405)$, $\eta(1470)$, $\eta(1760)$, $f_1(1285)$, $f_1(1420)$ and $h_1(1405)$ resonances. The $K^0_\mathrm{S} K\pi$ Dalitz plots are dominated by asymmetric crossing $K^* \bar{K}$ bands which are different for the two B^+ decay modes. This is due to a different interference pattern between the 1^{++} and 1^{+-} amplitudes in the two channels. Branching fractions are measured for each resonant contribution.

DOI: 10.1103/PhysRevD.111.092009

I. INTRODUCTION

Quantum chromodynamics (QCD) allows, in addition to mesons and baryons, the existence of exotic states such as glueballs, hybrids, and multiquark states. In particular, gluonium states have been extensively searched for over the past few decades in several processes such as radiative decays of charmonium, central production, $\bar{p}p$ annihilations, etc. [1]. The experimental confirmation of states having valence gluon content would provide fundamental information about QCD in the confinement regime and would be a direct test of QCD theory [2]. Significant progress on the experimental side has been made, but many issues remain unresolved [1,3]. In the sector of the pseudoscalar glueball [4], phenomenological models [5–7] calculate a mass around 1.4 GeV,[1] while lattice QCD calculations [2] predict a mass around 2.5 GeV. The difference in predicted masses is caused by the assumed effective gluon mass inside the hadrons [4].

One of the most interesting and disputed questions is the nature of the pseudoscalar structure with a mass around 1.4 GeV, the so-called "$\iota(1440)$" state. This was first observed in the early 1980s by the Mark II and Crystal Ball Collaborations [8,9] in the $K\bar{K}\pi$ final state using J/ψ radiative decays. A summary of the experimental and phenomenological status of the subject can be found in Ref. [10]. The structure has been subsequently confirmed by different experiments and is often interpreted as the combination of three states: two pseudoscalars, the $\eta(1405)$, $\eta(1475)$ and one axial state, the $f_1(1420)$ meson [11]. Pseudoscalar structures in the mass region below 2 GeV are also observed in the $\eta^{(\prime)}\pi\pi$ and VV (where V refers to ρ, ω vector mesons) final states [10]. Whether these observed pseudoscalar structures originate from the same source remains unclear. However, an amplitude analysis of $J/\psi \to \gamma\omega\omega$ decays by the BES experiment provides strong evidence of a pseudoscalar state, labeled as the $\eta(1760)$ [12]. Recently, the BESIII experiment has performed a high-yield partial-wave analysis of the $K^0_\mathrm{S} K^0_\mathrm{S} \pi^0$ system produced in radiative J/ψ decays [13], confirming the previously observed resonance composition of the structure around 1.4 GeV.

The $K^0_\mathrm{S} K\pi$ mass region below 1.6 GeV is further complicated by the presence of two $J^{PC} = 1^{++}$ states, $f_1(1420)$ and $f_1(1510)$, both potential candidates for the $s\bar{s}$ member of the $J^{PC} = 1^{++}$ nonet. The $f_1(1420)$ state is observed in $\pi^- p$ interactions and central production [14], while the $f_1(1510)$ resonance is mostly seen in $K^- p$ interactions [15,16]. In the latter, strong interference effects are observed between the $J^{PC} = 1^{++}$ $f_1(1510)$ and the

---

[*] Full author list given at the end of the article.

[1] Natural units with $\hbar = c = 1$ are used throughout this paper.

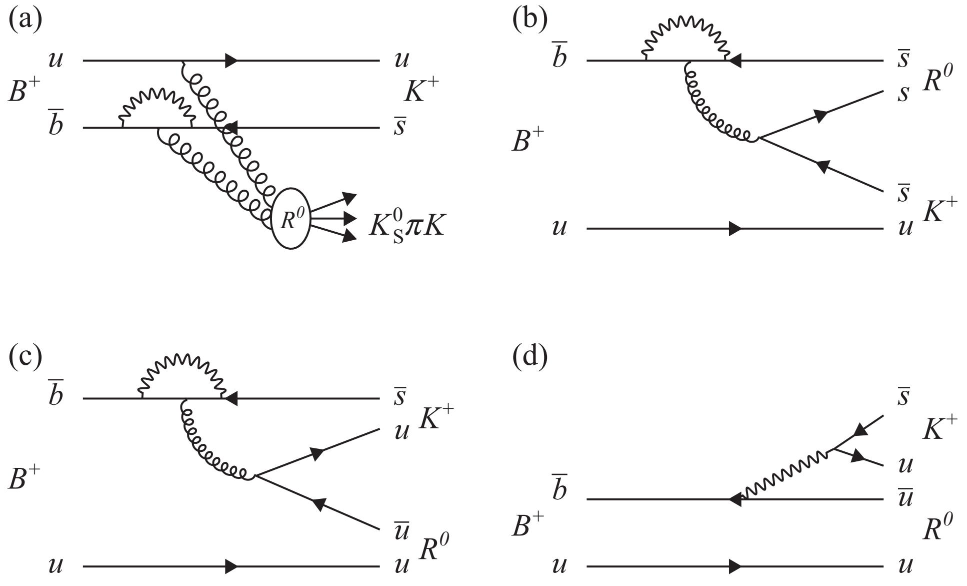

FIG. 1. Possible diagrams for B^+ decays involving the production of a resonance R^0 being (a) a gluonium state, (b) a $s\bar{s}$ meson, or (c), (d) an $u\bar{u}$ meson.

$J^{PC} = 1^{+-}$ $h_1(1415)$ states [15]. The presence of two $J^{PC} = 1^{++}$ states close in mass suggests the possibility that the $f_1(1420)$ could be a $K^*\bar{K}$ molecule [17].

In the present paper, a study of the $B^+ \to K_S^0 K^- \pi^+ K^+$ and $B^+ \to K_S^0 K^+ \pi^- K^+$ final states is presented.[2] These decays can proceed through different diagrams, as shown in Fig. 1. Decays of B mesons to final states with strangeness have been proposed as potential channels for searching for gluonium states [18]. A possible diagram for the production of a gluonium state R^0 decaying to $K_S^0 K\pi$ is shown in Fig. 1(a). However, in the same B decays, contributions from $s\bar{s}$ and $u\bar{u}$ resonances are also expected [see Figs. 1(b)–1(d)]. Possible diagrams describing the $B^+ \to K_S^0 K^- \pi^+ K^+$ and $B^+ \to K_S^0 K^+ \pi^- K^+$ nonresonant decays are shown in Fig. 2. Note that the $K_S^0 K\pi$ system is charge-conjugated in the two B^+ decay modes.[3]

Very little is known at present about charmless B decays to pseudoscalar and axial meson resonances [19]. The *BABAR* Collaboration [20] has studied neutral resonances, referred to R^0 in the following, in the $B^+ \to R^0 K^+$ decays, where the R^0 mass spectra were interpreted as signals from $\eta(1475) \to K^*\bar{K}$ and $\eta(1295) \to \eta\pi^+\pi^-$.

II. DETECTOR, DATA AND SIMULATION

The LHCb detector [21,22] is a single-arm forward spectrometer covering the pseudorapidity range $2 < \eta < 5$, designed for the study of particles containing b or c quarks. The detector elements particularly relevant to this analysis are a silicon-strip vertex detector (VELO) [23] surrounding the pp interaction region that allows c and b hadrons to be identified by exploiting their characteristically long flight distance; a tracking system that provides a measurement of the momentum, p, of charged particles; and two ring-imaging Cherenkov detectors that are able to discriminate between different species of charged hadrons. Photons, electrons and hadrons are identified by a calorimeter system consisting of scintillating-pad and preshower detectors, an electromagnetic and a hadronic calorimeter. Muons are identified by a system composed of alternating layers of iron and multiwire proportional chambers.

The analysis is performed on pp collisions data at center-of-mass energies 7, 8 and 13 TeV collected by the LHCb experiment during Runs 1 and 2 and corresponding to an integrated luminosity of 9 fb^{-1}. The online event selection is performed by a trigger [24], which consists of a hardware stage, based on information from the calorimeter and muon systems, followed by a software stage, which applies a full event reconstruction. During offline selection, trigger signatures are associated with reconstructed particles. Since the trigger system uses the transverse momentum of the charged particles with respect to the beam axis, p_{T}, the phase-space and time acceptance is different for events where signal tracks were involved in the trigger decision and those where the trigger decision was made using information from the rest of the event only. Data from both trigger conditions are used but studied separately for consistency tests and for the evaluation of systematic uncertainties.

Simulation is required to model the effects of the detector acceptance and the applied selection requirements. In the

---

[2] The inclusion of charge-conjugate processes is implied throughout the paper.

[3] Kaons and pions charges are not indicated when the sentence refers to both B^+ decay modes.

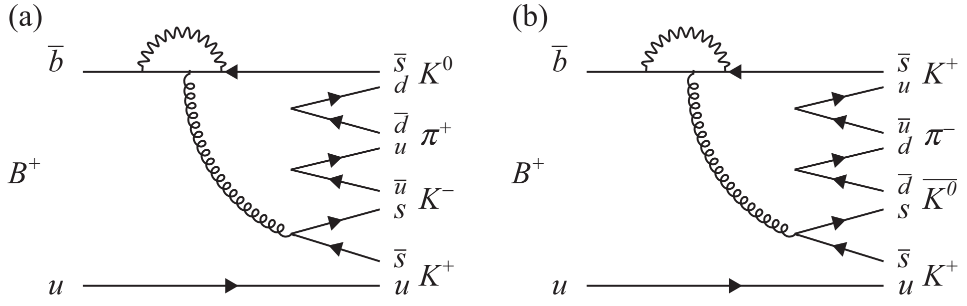

FIG. 2. Possible diagrams describing (a) $B^+ \to K^0 K^- \pi^+ K^+$ and (b) $B^+ \to \bar{K}^0 K^+ \pi^- K^+$ nonresonant decays.

simulation, pp collisions are generated using PYTHIA [25] with a specific LHCb configuration [26]. Decays of unstable particles are described by EvtGen [27], in which final-state radiation is generated using PHOTOS [28]. The interaction of the generated particles with the detector, and its response, are implemented using the Geant4 toolkit [29] as described in Ref. [30]. In the simulation, B^+ meson decays are modeled according to a phase-space distribution.

III. EVENT SELECTION

This paper presents a study of the two B^+ decay modes, $B^+ \to (K^0_S K^- \pi^+) K^+$ and $B^+ \to (K^0_S K^+ \pi^-) K^+$ [31], in the region of $m(K^0_S K\pi) < 1.85$ GeV. Candidate K^0_S mesons are reconstructed via their decay into the $\pi^+\pi^-$ final state, classified into two categories. The first includes K^0_S mesons that decay early enough for the pions to be reconstructed within the VELO, referred to as long K^0_S ($K^0_{\rm SLL}$). The second category includes K^0_S mesons that decay later, resulting in pion track segments that lie outside the VELO, referred to as downstream K^0_S ($K^0_{\rm SDD}$). While the $K^0_{\rm SLL}$ category has better mass, momentum and vertex resolution, the number of $K^0_{\rm SDD}$ candidates is approximately twice as large.

Candidate B^+ mesons are formed by combining the K^0_S candidate with three additional charged tracks. A kinematic fit of the entire decay tree is performed [32], under the assumption that the B^+ candidate originates from a good-quality primary vertex. The selection of K^0_S and B^+ candidates requires appropriate particle-identification information for each track and imposes broad invariant-mass selections around the known K^0_S and B^+ masses [19].

To suppress background contribution, in particular the combinatorial background formed from random combinations of unrelated tracks, the candidates satisfying the trigger requirements are filtered by a loose selection, followed by a multivariate analysis optimized separately for each final state. The selection criteria are tuned to minimize correlation of the signal efficiency with the kinematic variables, resulting in better control of the corresponding systematic uncertainties. As a result, the selection relies minimally on the kinematics of the final-state particles and instead focuses on the topological features associated with the detached vertex of the B^+ candidate. These features include the impact parameters of the B^+ candidate and its decay products, the fit quality of the decay vertices of the B^+ and K^0_S candidates, and the separation of these vertices from each other and from the primary vertex.

The separation of signal from combinatorial background is achieved by means of a boosted decision tree (BDT) classifier [33,34], implemented within the TMVA toolkit [35]. For this analysis a BDT with a gradient boosting algorithm [36] is used, with separate classifiers for the $K^0_{\rm SLL}$ and $K^0_{\rm SDD}$ categories.

Although the amplitude analysis is performed for $m(K^0_S K\pi) < 1.85$ GeV (see Sec. V), to obtain information on the resonant contribution in an extended mass region, the classifiers are trained using data and simulated signal decays with $m(K^0_S K\pi) < 2.5$ GeV from both B^+ decay modes. The simulation matches the relative yields of the dataset at the various center-of-mass energies. It is assumed that the efficiencies for the reconstruction of the $B^+ \to K^0_S K^- \pi^+ K^+$ and $B^+ \to K^0_S K^+ \pi^- K^+$ decays are the same. Data from the lower and upper mass sidebands of the B^+ signal region are used as background proxy in the BDT training, as indicated in Fig. 3. The composition of the background sample reflects the data-taking conditions, and events from the sidebands from both B^+ decays are included in equal proportions. The optimization of the BDT-classifier working point is performed by considering the figure of merit

$$S = \frac{N_{\rm sig}}{\sqrt{N_{\rm sig} + N_{\rm bkg}}}, \qquad (1)$$

where $N_{\rm sig}$ and $N_{\rm bkg}$ represent the B^+ signal, respectively, in the signal region and combinatorial background yield in the signal region evaluated by fitting the $m(K^0_S K\pi K)$ mass distributions.

In order to facilitate the extraction of the K^0_S and B^+ signal and combinatorial background components from these invariant-mass spectra, a kinematic fit of the decay without constraints on the masses of the K^0_S and B^+ is

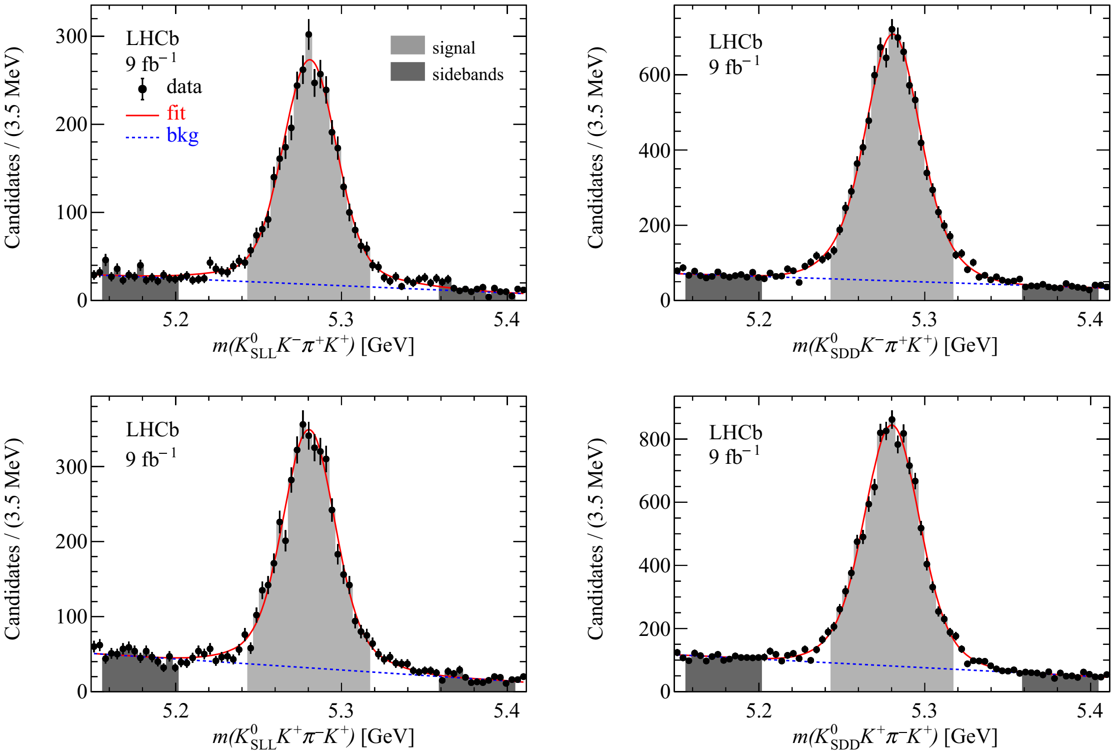

FIG. 3. Distributions of the (top) $K^0_{\rm S}K^-\pi^+K^+$ and (bottom) $K^0_{\rm S}K^+\pi^-K^+$ invariant mass for (left) $K^0_{\rm SLL}$ and (right) $K^0_{\rm SDD}$ candidates.

performed. The binned $\pi^+\pi^-$ invariant-mass distributions for $K^0_{\rm SLL}$ and $K^0_{\rm SDD}$ candidates are fitted separately. The fit model uses the sum of two Gaussian functions sharing the same mean for the signal and a linear function for the background. An effective resolution is computed as

$$\sigma_{\rm eff} = f\sigma_1 + (1-f)\sigma_2, \tag{2}$$

where σ_1 and σ_2 indicate the width of the two Gaussian functions and f is the fraction of the first Gaussian contribution. The resulting effective resolutions are $\sigma_{\rm eff} = 2.5$ MeV and $\sigma_{\rm eff} = 6.5$ MeV for the LL and DD categories, respectively. The $K^0_{\rm S}$ signals are selected within $3.0\sigma_{\rm eff}$ of the fitted $K^0_{\rm S}$ mass of 497.8 MeV.

To improve the resolution of the other invariant masses, the energy of the selected candidate $K^0_{\rm S}$ is calculated as

$$E_{K^0_{\rm S}} = \sqrt{p^2_{K^0_{\rm S}} + m^2_{K^0_{\rm S}}}, \tag{3}$$

where $p_{K^0_{\rm S}}$ is the reconstructed $K^0_{\rm S}$ momentum and $m_{K^0_{\rm S}}$ the known $K^0_{\rm S}$ mass [19]. Compared to using the $K^0_{\rm S}$ mass constraint, this method achieves the same resolution for the $K^0_{\rm S}K\pi K$ invariant mass but results in a slightly worse resolution, by ~6%, for the $K^0_{\rm S}K\pi$ invariant mass. However, it retains the ability to extract both the B^+ and $K^0_{\rm S}$ signals and the combinatorial background from a fit to the $K^0_{\rm S}K\pi K$ and $\pi^+\pi^-$ invariant-mass spectra.

Particle identification of the three charged hadrons is performed using the output of a neural network (NN) trained on the information of all the relevant subdetectors. The figures of merit are expressed as $P_K = NN_K(1-NN_\pi)$ for kaon identification and $P_\pi = NN_\pi(1-NN_K)$ for pion identification, where NN_π and NN_K are the NN probabilities for pion and kaon identification, respectively. Very loose selections are applied to these quantities to maximize the significance of the B^+ candidate invariant-mass peak as a function of P_K or P_π. Tests performed using a large $\eta_c \to K^0_{\rm S}K\pi$ sample [31] show that $(0.35 \pm 0.05)\%$ and $(3.0 \pm 0.1)\%$ of η_c signal decays are removed from both B^+ decays under the pion and kaon hypotheses, respectively. This procedure ensures that minimal bias is introduced into the angular distributions of the B^+ decays. With such particle-identification requirements it is found that data and simulation agree, in fractional η_c losses, within 2 standard deviations (σ).

Figure 3 shows the $K^0_{\rm S}K^-\pi^+K^+$ and $K^0_{\rm S}K^+\pi^-K^+$ invariant-mass spectra for the selected candidates, separated by $K^0_{\rm SLL}$ and $K^0_{\rm SDD}$ categories. The fits give a signal peak B^+-mass value of 5280.0 MeV and an effective width of $\sigma_{\rm eff} = 17.7$ MeV. Signal candidates are selected in a window of $\pm 2\sigma_{\rm eff}$ (used in the amplitude analysis reported in Sec. V) of the fitted B^+ mass, common to the four datasets. Table I lists the fitted yields and purities (P) in the B^+ signal region for the different datasets, where the purity is defined as

TABLE I. Fitted B^+ signal yield and purity for $K^0_SK^-\pi^+K^+$ and $K^0_SK^+\pi^-K^+$ final states separated by K^0_S type.

Final state	B^+ signal yield	B^+ purity [%]
$K^0_SK^-\pi^+K^+$		
K^0_{SLL}	2911 ± 68	87.1 ± 0.6
K^0_{SDD}	7672 ± 116	87.7 ± 0.4
$K^0_SK^+\pi^-K^+$		
K^0_{SLL}	3497 ± 86	83.5 ± 0.6
K^0_{SDD}	8955 ± 112	83.7 ± 0.4

$$P = \frac{N_{\rm sig}}{N_{\rm sig} + N_{\rm bkg}}. \tag{4}$$

It is found that P, for the four datasets, does not depend on the collision energy nor the data-taking conditions, which simplifies the amplitude analysis and they are analyzed together. Approximately 0.02% of the events contain multiple B^+ decay candidates, all of which are retained for further analysis.

The $K^0_SK\pi$ invariant-mass spectra for events in the B^+ signal region, summed over the K^0_{SLL} and K^0_{SDD} datasets, are shown in Fig. 4. The lower and upper mass sidebands around the B^+ signal peak, representing the background, defined in the ranges $[-6\sigma_{\rm eff}, -4\sigma_{\rm eff}]$ and $[4\sigma_{\rm eff}, 6\sigma_{\rm eff}]$, are superimposed onto the $K^0_SK\pi$ invariant-mass spectrum from the B^+ signal region. For the $B^+ \to K^0_SK^+\pi^-K^+$ final state, which has two kaons with the same charge, the smallest of the two possible mass combinations is plotted. Notably, for $m(K^0_SK\pi) < 2.3$ GeV, there is only one combination possible.

The $K^0_SK\pi$ mass spectra show a peak at the position of the $f_1(1285)$ resonance, followed by a broad enhancement suggesting the presence of several states. A $D^0 \to K^0_SK\pi$ peak is visible, originating from the open-charm decay $B^+ \to \bar{D}^0K^+$. The structure above 1.9 GeV, which appears only in the background samples, is due to reflections from $D^0 \to K^0_S\pi^+\pi^-$ decays, where one pion is misidentified as a kaon. This D^0 background contribution has two different sources: (a) $B^+ \to \bar{D}^0\pi^+$ and (b) D^0 open-charm production in the background. The B^+ contribution is reconstructed by assigning the pion mass to both kaon candidates and selecting the candidate if the recalculated masses fall within mass windows around the D^0 and B^+ masses. The contribution (b) is reconstructed after having enhanced the D^0 signal by requiring the $K^0_S\pi^\pm$ mass to be in the $K^{*\pm}$ mass region. The combination of these two selections is illustrated by the black distributions shown in Fig. 4. This contribution is subsequently removed from the sideband sample.

IV. MASS RESOLUTION, EFFICIENCY AND BACKGROUND

The $K^0_SK\pi$ mass resolution is obtained from simulation as the difference between true and reconstructed mass in slices of the $K^0_SK\pi$ mass. The resolution is described by the sum of two Gaussian functions, with $\sigma_{\rm eff}$ [see Eq. (2)] varying across the $K^0_SK\pi$ invariant-mass values range $1.3 < m(K^0_SK\pi) < 1.9$ GeV. For K^0_{SLL} candidates $\sigma_{\rm eff}$ spans from 4.5 to 7.0 MeV, while for K^0_{SDD} candidates it ranges from 5.5 to 9.0 MeV. Since the width of the resonances present in this mass range is much larger than the experimental resolution, its effect is ignored. An exception is the $f_1(1285)$ resonance, whose description is discussed in Sec. VI A.

Several angular variables are used to show projected distributions and determine the efficiency profiles. The B^+ decay can be described by the process

$$B \to (K^0_SK\pi)K_4, \tag{5}$$

where K indicates the kaon participating in resonant decay to the $K^0_SK\pi$ system, with $m(K^0_SK\pi) < 1.85$ GeV, and K_4 is the spectator kaon.

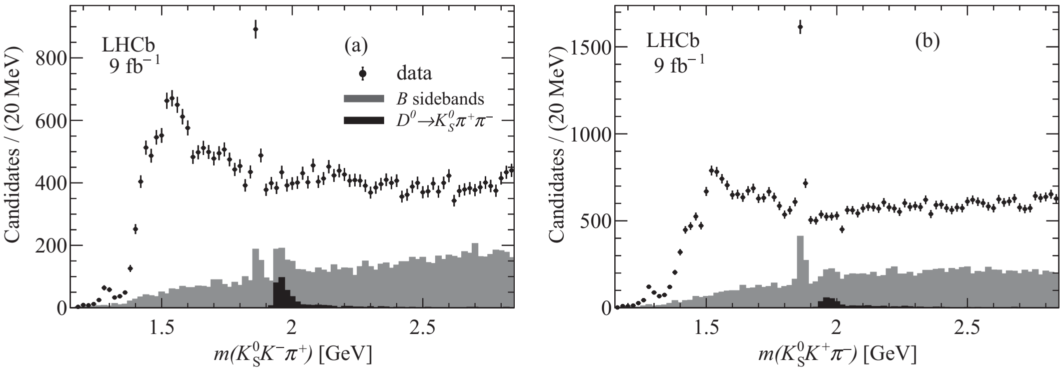

FIG. 4. $K^0_SK\pi$ invariant-mass distributions for (a) $B^+ \to K^0_SK^-\pi^+K^+$ and (b) $B^+ \to K^0_SK^+\pi^-K^+$ candidates in the B^+ signal region. The gray distributions are obtained from the B^+ mass sidebands normalized to the expected background in the signal region; the black distributions show the $D^0 \to K^0_S\pi^+\pi^-$ reflection from pions misidentified as kaons.

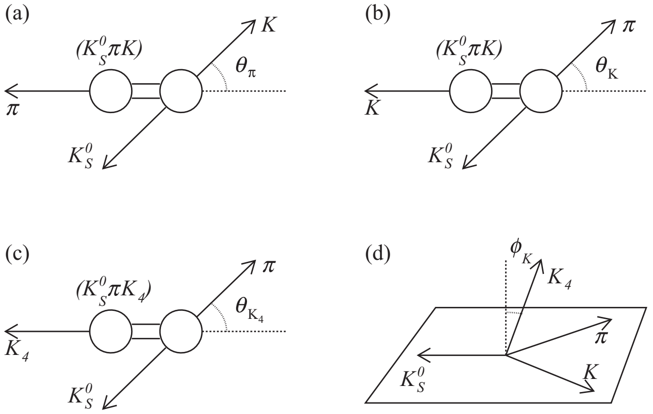

FIG. 5. Diagrams illustrating the angular variables θ_π, θ_K, θ_{K_4} and ϕ_K.

The angular distributions used in this analysis are defined as follows and illustrated in Fig. 5. The angle $\theta_\pi(\theta_K)$ is defined as the angle between the $K(\pi)$ in the $K^0_S K(K^0_S\pi)$ rest frame and the $K^0_S K(K^0_S\pi)$ direction in the $K^0_S K\pi$ rest frame. Similarly, the angle θ_{K_4} is defined by exchanging K with K_4. Finally, ϕ_K is the angle formed by the spectator K_4 momentum with the normal to the $K^0_S K\pi$ decay plane.

A. Efficiency

The kinematics of a four-body decay are fully described by five independent variables. A mixture of invariant-mass combinations and decay angles is used as variables in this analysis. The various possible invariant-mass combinations have different kinematic bounds; therefore, mass-reduced variables are used instead as they always range between 0 and 1. They are defined as [37]

$$m_x = \frac{1}{\pi}\arccos\left(2\frac{m - m_{\min}}{m_{\max} - m_{\min}} - 1\right), \tag{6}$$

where m, $m_{\min}$ and $m_{\max}$ indicate the invariant-mass and its minimum and maximum kinematically allowed values, respectively. Note that the m_x ranges are reduced by the request $m(K^0_S K\pi) < 1.85$ GeV.

Two types of efficiencies are evaluated, total and local. The total efficiency describes the effects of the reconstruction on the full phase space of the B^+ decay to the four-body final state. Local efficiencies are evaluated in the specific $K^0_S K\pi$ mass region considered in the present analysis. The efficiencies are evaluated using simulated samples that undergo the same reconstruction and selection criteria as the data. Efficiency distributions are determined by taking the ratio of selected to generated events, projected onto the relevant kinematic variables. A comparison of the p_T distributions of B^+ candidates between simulation and data shows a small disagreement, which is corrected by weighting the former to match the latter.

The total efficiency for the two B^+ decay modes is evaluated in an iterative manner as described in Ref. [31]. The local efficiency is evaluated separately for $K^0_{\rm SLL}$ and $K^0_{\rm SDD}$ simulations using the same method.

First, the variable whose efficiency distribution shows the most significant deviation from uniformity, $m_x(K^0_S K_4)$, is identified. Figure 6 shows the efficiency projected onto $m_x(K^0_S K_4)$ separately for the $K^0_{\rm SLL}$ and $K^0_{\rm SDD}$ samples and the result of a fit with a seventh-order polynomial function, labeled as $\epsilon_1(m_x(K^0_S K_4))$. The simulated candidates are then weighted by the inverse of the efficiency $1/\epsilon_1(m_x(K^0_S K_4))$ and a second variable $(m_x(K^0_S K))$ is chosen and fitted with a fifth-order polynomial function, labeled as $\epsilon_2(m_x(K^0_S K))$. The events are then weighted by the factor $1/(\epsilon_1(m_x(K^0_S K_4))\cdot\epsilon_2(m_x(K^0_S K)))$. The process continues in this fashion, terminating when the efficiency is consistent with being uniform across all nine of the considered variables [$m(K^0_S K\pi)$, five two-body $m_x(K^0_S\pi(K))$ combinations and the three angular variables, $\cos\theta_K$, $\cos\theta_{K^0_S}$ and $\cos\phi$] both in their one- and two-dimensional projections. The total efficiency for each K^0_S category, $\epsilon_{\rm LL}$ and $\epsilon_{\rm DD}$, is found to be well described by the following functions:

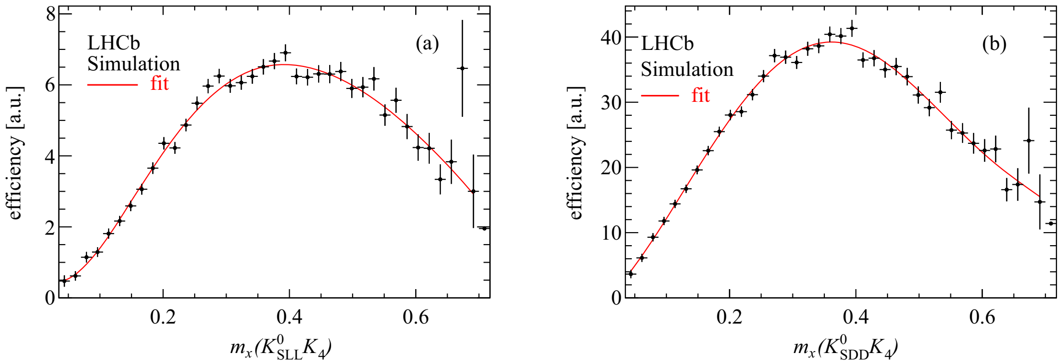

FIG. 6. Efficiency projections (in arbitrary units) on $m_x(K^0_S K_4)$ for the (a) $K^0_{\rm SLL}$ and (b) $K^0_{\rm SDD}$ samples with $m(K^0_S K\pi) < 1.85$ GeV.

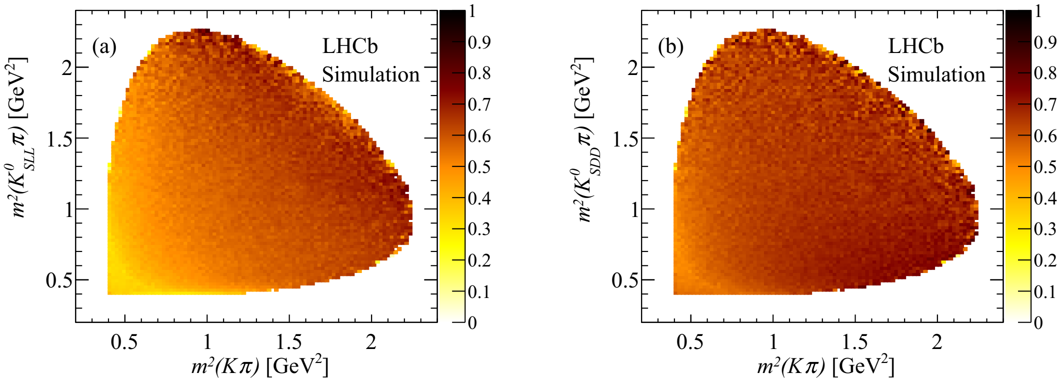

FIG. 7. Two-dimensional efficiency distributions given in arbitrary units in the $m(K^0_SK\pi) < 1.85$ GeV mass region for the (a) $K^0_{\rm SLL}$ and (b) $K^0_{\rm SDD}$ samples.

$$\epsilon_{\rm LL} = \epsilon_1(m_x(K^0_SK_4))\cdot\epsilon_2(m_x(K^0_SK))\cdot\epsilon_3(\cos\phi)\cdot\epsilon_4(m_x(K^0_S\pi)),$$
$$\epsilon_{\rm DD} = \epsilon_1(m_x(K^0_SK_4))\cdot\epsilon_2(m_x(K^0_SK))\cdot\epsilon_3(\cos\phi). \quad (7)$$

Figure 7 shows the resulting efficiency distributions across the Dalitz plot for $m(K^0_SK\pi) < 1.85$ GeV while Fig. 8 shows the normalized efficiency projected onto $\cos\phi$ and $\cos\theta_\pi$.

B. Description of the background

The background distribution is obtained by inspecting the B^+ mass sidebands where the $K^0_{\rm SLL}$ and $K^0_{\rm SDD}$ data are combined and performing an unbinned maximum-likelihood fit to the $K^0_SK\pi$ and two-body mass distributions. The $K^0_SK\pi$ mass distribution is described by a fourth-order polynomial function, while the two-particle mass distributions are modeled including the contributions from charged and neutral $K^*(892)$ resonances with parameters fixed to known values [19], and a nonresonant contribution. The former are modeled with relativistic Breit-Wigner (BW) functions, while the latter is represented by a constant value. In the following $K^*_{\rm ne}(892)$ and $K^*_{\rm ch}(892)$ indicate the neutral and charged $K^*(892)$ contributions, respectively.

Figure 9 shows the $K^0_SK\pi$ mass spectra of the B^+ sidebands along with the result from the fits. The two-particle mass distributions and fits results are shown in Fig. 10, with the fit results listed in Table II.

V. AMPLITUDE ANALYSIS

Figure 11 shows the $K^0_SK\pi$ Dalitz plot in the $1.30 < m(K^0_SK\pi) < 1.85$ GeV mass region, separately for $B^+ \to K^0_SK^-\pi^+K^+$ (10,830 candidates) and $B^+ \to K^0_SK^+\pi^-K^+$ (12,930 candidates). The distributions are dominated by two intersecting bands associated with the $K^*_{\rm ne}(892)$ and $K^*_{\rm ch}(892)$ resonances. Notably, the event distribution along the bands is not uniform, due to the spin of the contributing resonances and their interference. A comparison between

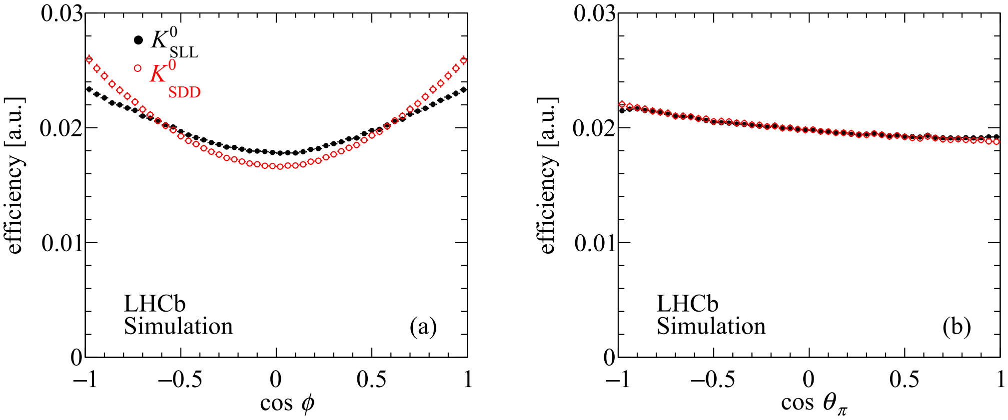

FIG. 8. Normalized efficiency distributions from simulation in the $m(K^0_SK\pi) < 1.85$ GeV mass region projected onto (a) $\cos\phi$ and (b) $\cos\theta_\pi$ for the $K^0_{\rm SLL}$ and $K^0_{\rm SDD}$ samples.

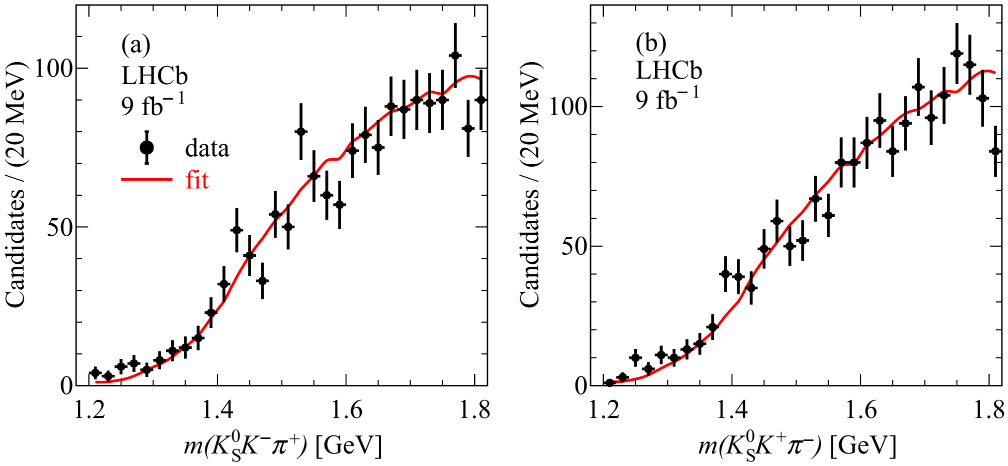

FIG. 9. Distribution of the $K^0_SK\pi$ mass of background candidates from the B^+ mass sidebands for (a) $B^+ \to K^0_SK^-\pi^+K^+$ and (b) $B^+ \to K^0_SK^+\pi^-K^+$ decays.

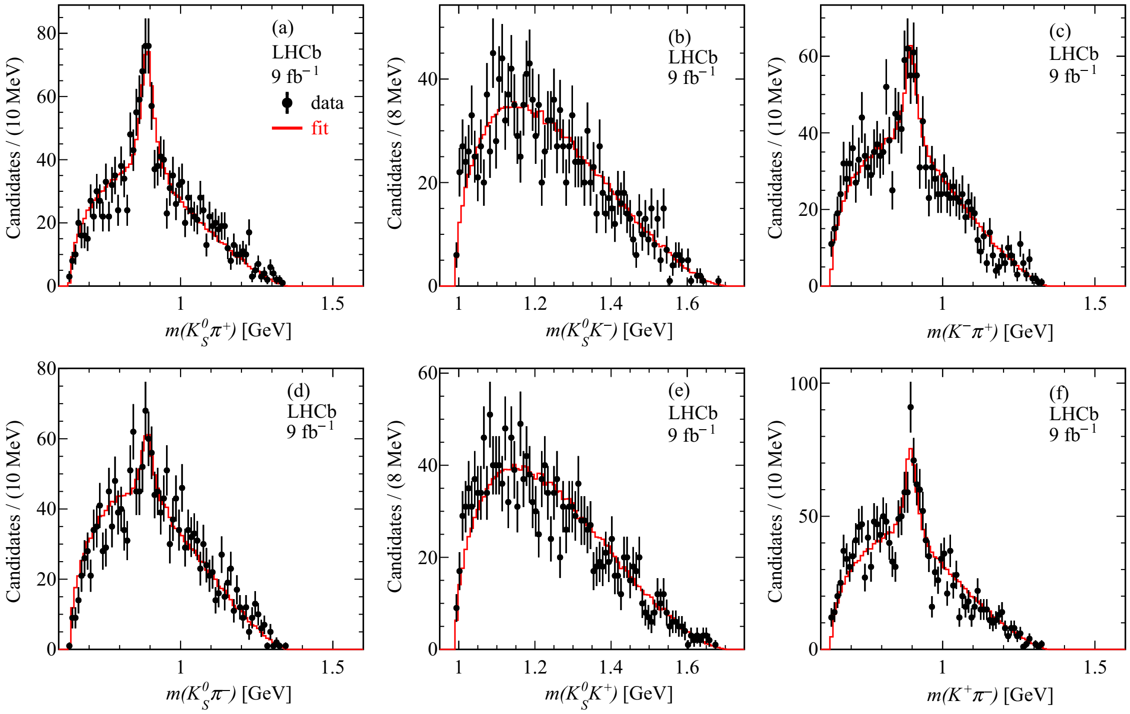

FIG. 10. Two-particle mass distributions of the background candidates in the B^+ mass sidebands with the result of the fit also shown for (a)–(c) $K^0_SK^-\pi^+K^+$ and (d)–(f) $K^0_SK^+\pi^-K^+$ decays.

the $B^+ \to K^0_SK^-\pi^+K^+$ and $B^+ \to K^0_SK^+\pi^-K^+$ data reveals opposite behavior in the interference pattern between the $K^*_{\mathrm{ne}}(892)$ and $K^*_{\mathrm{ch}}(892)$ bands.

A. Fitting method

An amplitude analysis of $B^+ \to K^0_SK^-\pi^+K^+$ and $B^+ \to K^0_SK^+\pi^-K^+$ decays is performed with two unbinned maximum-likelihood fits, one for each decay channel. The likelihood function is defined as

$$\mathcal{L} = \prod_{n=1}^{N}\left[P\epsilon(\vec{y}_n)\frac{\sum_{i,j}c_ic_j^*A_i(\vec{x}_n)A_j^*(\vec{x}_n)}{\sum_{i,j}c_ic_j^*I_{A_iA_j^*}} + (1-P)\frac{\sum_k f_kB_k(\vec{z}_n)}{\sum_k f_kI_{B_k}}\right], \tag{8}$$

where N is the number of events in the B^+ signal region and P is the signal purity listed in Table I; $\epsilon(\vec{y}_n)$ is the efficiency parametrized as described in Sec. IV A in terms of the list of mass-reduced variables, here indicated by $\vec{y}_n$; the $A_i(\vec{x}_n)$

TABLE II. Yields and fractional composition of the background from a fit to the candidates in the B^+ mass sidebands for $K^0_{\rm S}K^-\pi^+K^+$ and $K^0_{\rm S}K^+\pi^-K^+$ decays.

Final state	Candidates	$K^*_{\rm ne}(892)$	$K^*_{\rm ch}(892)$	Nonresonant
$K^0_{\rm S}K^-\pi^+K^+$	1702	0.110 ± 0.016	0.177 ± 0.018	0.713 ± 0.025
$K^0_{\rm S}K^+\pi^-K^+$	1933	0.126 ± 0.016	0.073 ± 0.016	0.801 ± 0.022

function, modeled by the nonrelativistic Zemach-tensor formalism [38–40], described in Appendix A and listed in Table XV, describes the complex signal-amplitude contribution parametrized as a function of the list of parameters $\vec{x}_n$. The parameter c_i is the complex coefficient for the ith signal component, which is allowed to vary in the fit. One amplitude, the largest, is taken as the reference by setting $|c_i| = 1$ with zero phase. The term $B_k(\vec{z}_n)$ represents the background probability-density function, described in terms of the parameters $\vec{z}_n$ as discussed in Sec. IV B. It is assumed that interference between signal and background amplitudes can be ignored. The parameter f_k is the magnitude of the kth background component, obtained from the fit to the candidates in the sideband regions as described in Sec. IV B. The terms $I_{A_iA_j^*} = \int A_i(\vec{x})A_j^*(\vec{x})\epsilon(\vec{y})\mathrm{d}\vec{x}\mathrm{d}\vec{y}$ and $I_{B_k} = \int B_k(\vec{z})\mathrm{d}\vec{z}$ are normalization integrals. They are determined through numerical integration on phase-space-generated events, with initial-state masses for the signal and background samples set according to their respective distributions measured from the B^+-candidate mass. The $K^0_{\rm SLL}$ and $K^0_{\rm SDD}$ datasets enter in the likelihood function according to their efficiency and purity.

For each contribution, resonant or nonresonant, the fraction is defined as

$$f_i = \frac{|c_i|^2 \int |A_i(\vec{x})|^2 \mathrm{d}\vec{x}}{\int |\sum_j c_j A_j(\vec{x})|^2 \mathrm{d}\vec{x}}. \qquad (9)$$

The fractions f_i do not necessarily sum to 100% because of interference effects. The uncertainty of each f_i is evaluated by propagating the covariance matrix obtained from the fit. Interference fractions are evaluated as

$$f_{ij} = \frac{\int 2\mathcal{R}e[c_i c_j^* A_i(\vec{x})A_j^*(\vec{x})]\mathrm{d}\vec{x}}{\int |\sum_j c_j A_j(\vec{x})|^2 \mathrm{d}\vec{x}}. \qquad (10)$$

To evaluate the quality of the fit, a large simulated sample is prepared, where events are generated uniformly in the phase space [41]. These events are weighted by the fitted likelihood function, normalized to the yields in data and compared to the data distribution on several invariant-mass and angular projections. Several two-dimensional distributions are divided into a grid of $n \times n$ cells. In total $N_{\rm cells}$ cells are considered whose weighted yield is at least two. A χ^2 estimator is used, defined as

$$\chi^2 = \sum_{i=1}^{N_{\rm cells}} (N^i_{\rm obs} - N^i_{\rm exp})^2/\sigma^2, \qquad (11)$$

where $N^i_{\rm obs}$ and $N^i_{\rm exp}$ are event yields from data and simulation, respectively. Here $\sigma \equiv \sqrt{N^i_{\rm exp}}$ for cells containing more than nine entries, while it is approximated as the average of the lower and upper Poisson uncertainties at the 68% confidence level for lower statistics cells. The figure of merit for the fit quality is defined as $\chi^2/\mathrm{n.d.f.}$, with $\mathrm{n.d.f.} = N_{\rm cells} - n_{\rm par} - 1$, where $n_{\rm par}$ is the number of free parameters and one degree of freedom is removed because of the normalization constraint.

VI. AMPLITUDE FIT

A. Study of the $f_1(1285)$ mass region

The $f_1(1285)$ state is a well-known resonance with established $J^P = 1^+$ quantum numbers. The resonance is

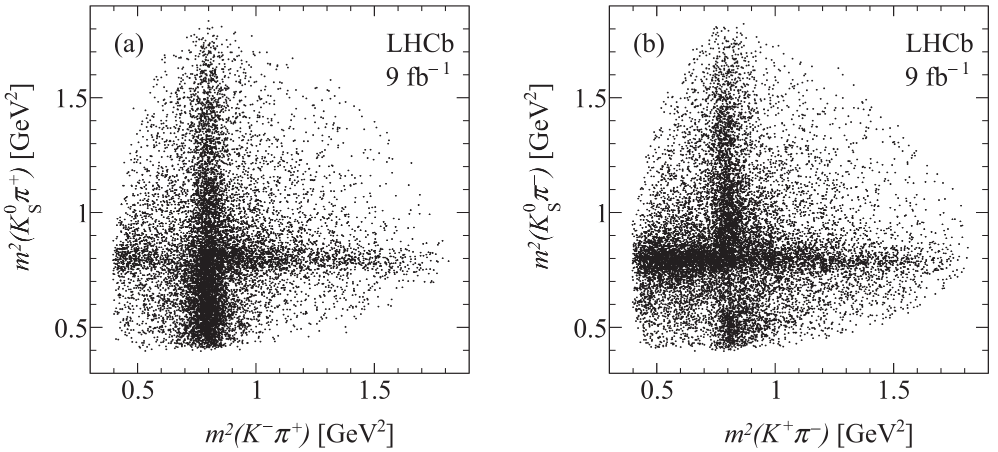

FIG. 11. Dalitz plot distribution of the $K^0_{\rm S}K\pi$ system for candidates with $1.30 < m(K^0_{\rm S}K\pi) < 1.85$ GeV for (a) $B^+ \to K^0_{\rm S}K^-\pi^+K^+$ and (b) $B^+ \to K^0_{\rm S}K^+\pi^-K^+$ decays.

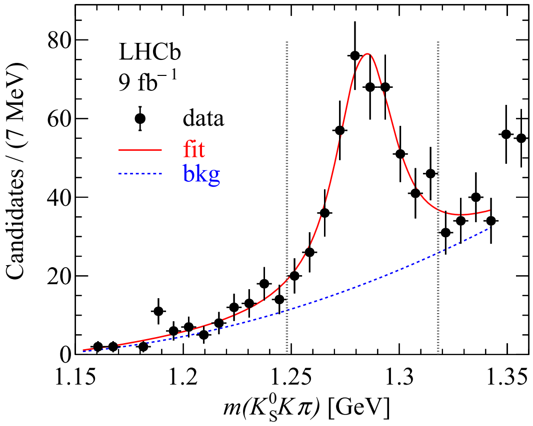

FIG. 12. Fit to the $m(K^0_S K\pi)$ mass distribution in the $f_1(1285)$ mass region with the result of the fit also shown. The dashed line indicates the fitted background; the vertical dotted lines indicate the region used for the amplitude analysis.

narrow and located in the threshold region of the $K^0_S K\pi$ phase space; therefore, little interference with other resonant amplitudes is expected. Therefore a study of this resonance allows to perform a simple test of the amplitude analysis model to correctly obtain a good description of the data and confirm the $f_1(1285)$ quantum numbers. The data from both B^+ decay modes are added as we do not expect significant differences. The $f_1(1285)$ decays to the $K^0_S K\pi$ final state mainly through the $a_0(980)\pi$ intermediate state [19], hereafter denoted as $a_0\pi$. Figure 12 shows the low-mass region of the $K^0_S K\pi$ spectrum, summed over the $K^0_{\rm SLL}$, $K^0_{\rm SDD}$, $B^+ \to K^0_S K^-\pi^+K^+$ and $B^+ \to K^0_S K^+\pi^-K^+$ data samples, where a significant $f_1(1285)$ signal is observed.

The data are fitted using the modulus squared of the BW function

$$\mathrm{BW}(m) = \frac{1}{(m_0 - m) - i\Gamma/2}, \tag{12}$$

where m indicates the $K^0_S K\pi$ mass, multiplied by a function representing the $K^0_S K\pi$ phase space for the signal and a second-order polynomial function for the background. Since the known width of the $f_1(1285)$ resonance, $\Gamma = 23.0 \pm 1.1$ MeV [19], is comparable with the average mass resolution in this region, $\sigma = 5.3$ MeV, the signal is alternatively modeled using a BW convolved with the experimental mass resolution fixed to this value. This fit is shown in Fig. 12 with the results from both fits summarized in Table III.

Both approaches yield similar-quality fits and results, though the width is larger without the BW convolution (see Table III). However, for simplicity, the BW model with no convolution is used to describe the $f_1(1285)$ line shape in the amplitude analysis described in Sec. VI B.

TABLE III. Results from the fits in the $f_1(1285)$ mass region.

Fitting method	χ^2/n.d.f.	m_0 [MeV]	Γ [MeV]	Yield
BW with resolution	13.3/22	1283.5 ± 1.5	27.4 ± 5.6	360 ± 50
BW	13.6/22	1283.5 ± 1.6	32.3 ± 5.4	381 ± 51

An amplitude analysis of the data in the $f_1(1285)$ mass region is performed by selecting candidates in the $1.248 < m(K^0_S K\pi) < 1.318$ GeV interval and combining the $B^+ \to K^0_S K^-\pi^+K^+$ and $B^+ \to K^0_S K^+\pi^-K^+$ data samples. This sample corresponds to 497 events and a B^+ purity of $P = 0.890 \pm 0.015$.

Three different hypotheses, listed in Table IV, are used to fit the data; in all cases the interference between the different contributions is included. In fit (a), the fit model consists of two contributions: $J^P = 1^+$ $f_1(1285) \to a_0(980)\pi$ and a phase-space (PS) contribution. In fit (b), the $f_1(1285)$ resonance is assumed to have quantum numbers $J^P = 0^-$. This hypothesis is discarded by the fit, having a much worse likelihood and χ^2/n.d.f. values. For (c) an additional $\eta(1295) \to a_0(980)\pi$ contribution is included. This gives a similar quality to fit (a) but returns large interference terms. The fraction of this additional contribution is 0.129 ± 0.050, consistent with zero within 2.6σ. Given the low significance and the large interference effects, fit (c) is discarded while fit (a) is considered as the baseline solution. These results are confirmed by the full amplitude analysis of the $K^0_S K\pi$ mass spectrum (see Sec. VI B). The fit projections, with comparisons between $J^P = 1^+$ and $J^P = 0^-$ $f_1(1285)$ assignments, are shown in Fig. 13.

To better visualize the difference between the two J^{PC} hypotheses, Fig. 14 shows the fit projections to the $\cos\theta_{K^0}$, $\cos\theta_\pi$ and $\cos\phi_K$ distributions. A significant discriminant power can be observed in the distribution of $\cos\phi_K$ due to the $f_1(1285)$ resonance originating from a B^+ decay.

The quoted χ^2/n.d.f. value listed in Table IV for the three different scenarios is obtained by dividing the Dalitz plot into a 10×10 grid and using the method described in Sec. V A.

B. Amplitude analysis of the full low-mass $K^0_S K\pi$ region

It is well known that the BW function provides a simplified description, strictly valid only in cases of isolated, single resonances, far away from thresholds. In the present analysis a particularly complex problem is faced, with the presence, in a limited mass region, of several interfering amplitudes with different quantum numbers. This approach, taking into account its limitations, is employed to describe the data in the present analysis.

An unbinned maximum-likelihood fit is performed to the data in the low-mass region $m(K^0_S K\pi) < 1.85$ GeV inserting all possible resonances which decay into the $K^0_S K\pi$ final state [19]. The $B^+ \to K^0_S K^-\pi^+K^+$ and $B^+ \to K^0_S K^+\pi^-K^+$ data are fitted separately. A search

TABLE IV. Results from the amplitude analysis of the $f_1(1285)$ mass region. Likelihood variations are evaluated with respect to the baseline fit (a). Positive changes in the $\Delta(-2\log\mathcal{L})$ means better results.

Amplitudes	$\Delta(-2\log\mathcal{L})$	Fractions	Sum of fractions	χ^2/n.d.f.
(a) $1^+ f_1(1285), PS$	$\cdots$	0.601 ± 0.042, 0.392 ± 0.042	0.993	$62/66 = 0.94$
(b) $0^- f_1(1285), PS$	-405.3	0.164 ± 0.041, 0.784 ± 0.104	0.948	$85/64 = 1.32$
(c) $1^+ f_1(1285), PS$, $0^-\eta(1295)$	19.7	0.577 ± 0.043, 0.766 ± 0.101 0.129 ± 0.050	1.471	$64/66 = 0.97$

for the best solution is performed by adding resonances one by one and considering as figures of merit the significance of their fit fractions, which relates to the increase of the likelihood and the decreasing χ^2/n.d.f.. Defining the significance of a given contribution $\sigma_R \equiv f/\delta_f$, where f and δ_f are the fitted fraction and the corresponding statistical error, contributions with $\sigma_R < 3$ are discarded. The list of resonances contributing to the two B^+ decay modes is given in Table V. In addition, a nonresonant phase-space contribution and incoherent $K^*_{\rm ne}(892)$ and $K^*_{\rm ch}(892)$ contributions are included, modeled by relativistic Breit-Wigner functions with no angular dependence. According to the results of Ref. [13], R^0 resonances are also allowed to decay directly to the $K^0_{\rm S}K\pi$ final state, here described by a constant term, neglecting a possible intermediate contribution from the $K^*_0(700)$ whose parameters are affected by large uncertainties [19].

Different fitting sequences are tried, taking as reference amplitude the $J^{PC} = 0^{-+}$ $\eta(1475) \to K^*\bar{K}$ or the $J^{PC} = 1^{++}$ $f_1(1420) \to K^*\bar{K}$, which are found to be significant in all the fits. Additional contributions are included and removed to test their significance and the effects on the fitting sequence. After finding the best solution, additional tests are performed to evaluate the

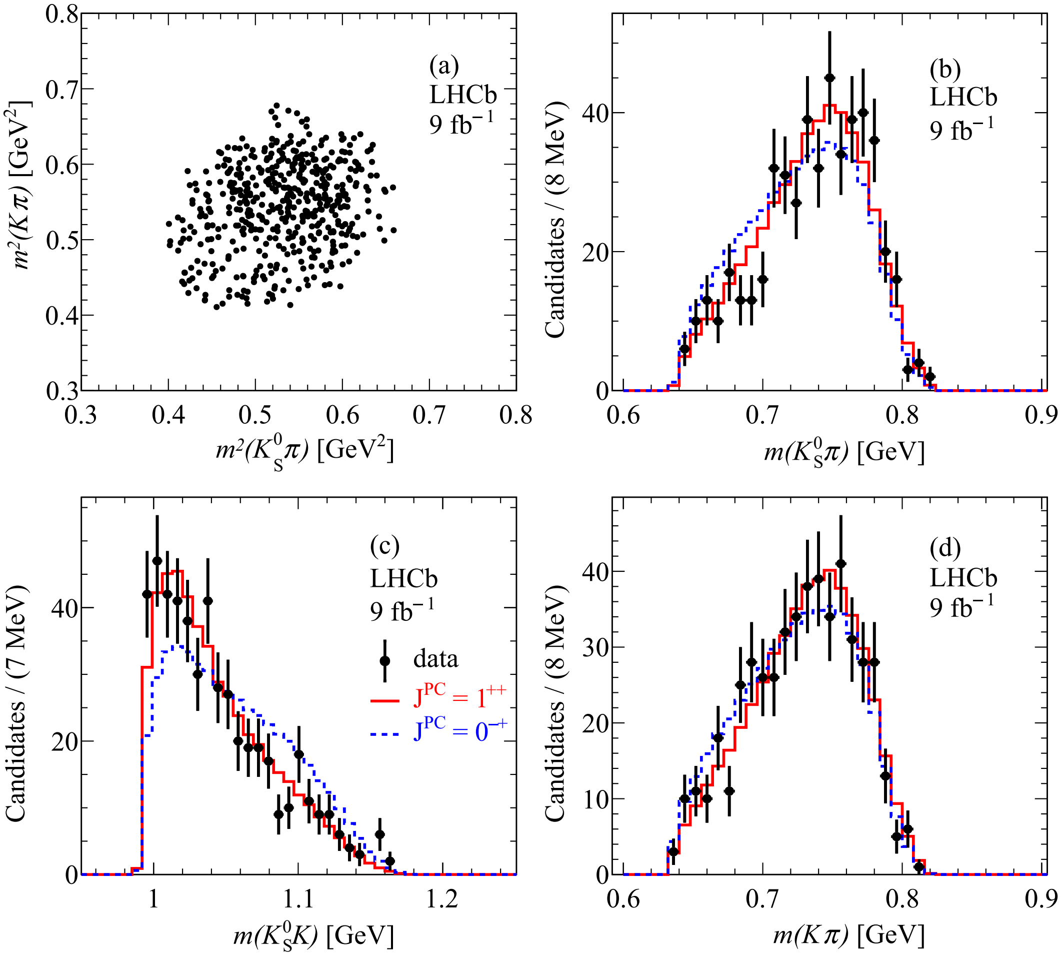

FIG. 13. (a) Dalitz plot of candidates in the $f_1(1285)$ mass region and (b)–(d) projections with the fit result also shown.

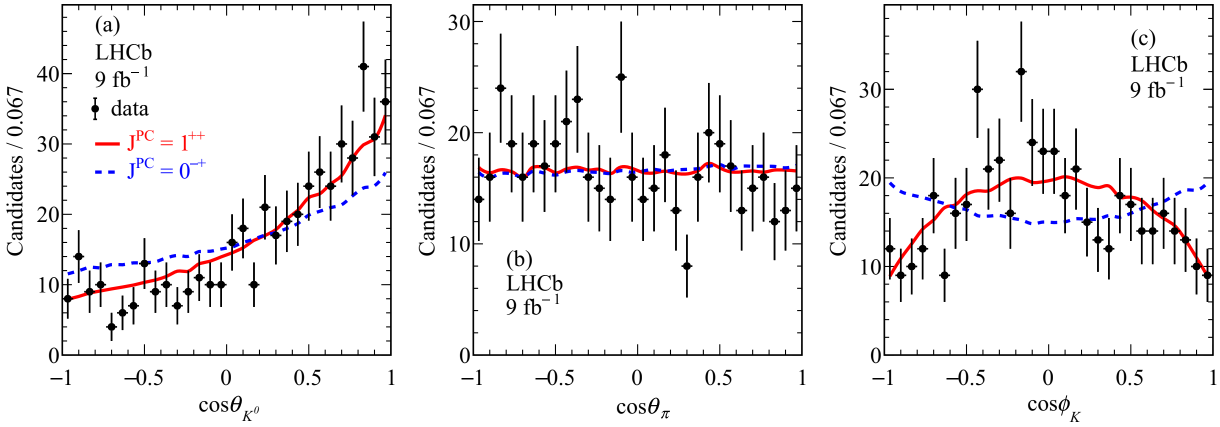

FIG. 14. Angular distributions in the $f_1(1285)$ mass region with fit projections corresponding to the two J^{PC} hypotheses.

significance of lower-level contributions. It is concluded that the baseline solution described below is unique and the list of resonances that describe the data is the same for both B^+ decay modes.

In the baseline fit, the amplitude for the $\eta(1475) \to K^*\bar{K}$ decay is used as a reference, with parameters fixed to the values of Ref. [13]. The fit-fraction and relative-phase results from the fits to the $B^+ \to K_S^0 K^- \pi^+ K^+$ and $B^+ \to K_S^0 K^+ \pi^- K^+$ data are summarized in Table VI.

TABLE V. List of the light-meson R^0 resonances which contribute to the B^+ decays studied. For the $\eta(1475)$ resonance both the PDG values [19] (in parentheses) and values from Ref. [13] are listed. For other resonances PDG values are shown. The $f_1(1285)$ width has been increased to 32.3 MeV to take into account the experimental resolution (see Sec. VI A). The decay products of the h_1 resonances can be in either a relative S or D wave (see Table XV).

Resonance	J^{PC}	m_0 [MeV]	Γ [MeV]	Decay mode
$\eta(1295)$	0^{-+}	1294.4 ± 4	55 ± 5	$a_0\pi$
$\eta(1405)$	0^{-+}	1408.8 ± 2	50.1 ± 2.6	$a_0\pi$ $K^*\bar{K}$ PS
$\eta(1475)$	0^{-+}	(1475 ± 4) 1507.6 ± 1.6	(90 ± 9) 115.8 ± 2.4	$a_0\pi$ $K^*\bar{K}$ PS
$\eta(1760)$	0^{-+}	1751 ± 15	240 ± 30	$a_0\pi$ $K^*\bar{K}$ PS
$f_1(1285)$	1^{++}	1281.9 ± 0.5	22.7 ± 1.1 (32.3)	$a_0\pi$
$f_1(1420)$	1^{++}	1426.3 ± 0.9	54.5 ± 2.6	$K^*\bar{K}$
$f_1(1510)$	1^{++}	1518 ± 5	73 ± 25	$K^*\bar{K}$
$h_1(1415)$	1^{+-}	1416 ± 8	90 ± 15	$K^*\bar{K}[S]$ $K^*\bar{K}[D]$
$h_1(1595)$	1^{+-}	1594 ± 15	384 ± 60	$K^*\bar{K}[S]$ $K^*\bar{K}[D]$
$\eta_2(1645)$	2^{-+}	1617 ± 5	181 ± 11	$a_0\pi$ $K^*\bar{K}$

The fits find the same resonance composition for both $B^+ \to K_S^0 K^- \pi^+ K^+$ and $B^+ \to K_S^0 K^+ \pi^- K^+$ decays and the results can be summarized as follows. The decay $B^+ \to R^0(\to K_S^0 K\pi)K^+$ is dominated by pseudoscalar $\eta(1405)$, $\eta(1475)$ and $\eta(1760)$ resonances, which contribute via the $K^*\bar{K}$, $a_0\pi$ and direct $K_S^0 K\pi$ decay modes. Contributions from $a_0(1450)\pi$ are tested but found consistent with zero. Significant contributions from the $J^{PC} = 1^{++}$ $f_1(1420)$ and $f_1(1510)$ resonances are also observed. Concerning the negative C-parity states, the $J^{PC} = 1^{+-}$ $h_1(1415)$ resonance is present in both S and D waves (see Table XV) as well as the $h_1(1595)$ resonance, which contributes only in the S-wave decay mode.

An attempt to include the $\eta(1295) \to a_0\pi$ contribution is made, but the significance σ_R is found to be below the threshold defined above. An $f_2'(1525)$ component is also included, but its fit fraction is consistent with zero as expected due to the very small branching fraction reported in Ref. [13]. Similarly, the presence of a $\phi(1680)$ resonance is tested but rejected by the fits to the data.

The sum of the fractions exceeds 100%, indicating the presence of interference effects. The majority of the interference terms are found to be very small. However, contributions with fractions greater than 5% are present and are mostly due to resonances decaying directly to $K_S^0 K\pi$ or via global PS contributions.

A comparison is made between the results obtained from the amplitude analyses of the two B^+ decays. This is achieved by introducing the significance $n\sigma_1$, defined as $\Delta f/\delta$, where Δf indicates the fraction difference and δ is the associated statistical uncertainty. A significance $n\sigma_2$ is also evaluated by replacing ϵ as the sum in quadrature of the statistical and systematic uncertainties. Similar quantities are defined for the evaluation of the significance of the phase difference $\Delta\phi$.

The results, summarized in Table VII, can be outlined as follows. Most of the fractional contributions are consistent between the two B^+ decay modes. A few fractional contributions have $n\sigma_1 > 5$ but with lower significances

TABLE VI. Results of the amplitude analysis for the two $B^+ \to R^0(\to K_S^0 K\pi)K^+$ final states. The parameters of the listed contributions are given in Table V.

		$B^+ \to K_S^0 K^- \pi^+ K^+$		$B^+ \to K_S^0 K^+ \pi^- K^+$	
Contribution	Decay	Fraction [%]	Phase [rad]	Fraction [%]	Phase [rad]
$\eta(1475)$	$K^*\bar{K}$	$10.7 \pm 1.1 \pm 1.1$	0	$10.3 \pm 1.1 \pm 1.4$	0
	$a_0\pi$	$1.4 \pm 0.4 \pm 0.4$	$3.18 \pm 0.19 \pm 0.15$	$1.8 \pm 0.4 \pm 0.4$	$2.92 \pm 0.14 \pm 0.13$
	PS	$15.2 \pm 2.1 \pm 2.1$	$3.33 \pm 0.10 \pm 0.12$	$8.9 \pm 1.4 \pm 2.7$	$3.57 \pm 0.11 \pm 0.13$
	Total	$27.4 \pm 2.4 \pm 2.4$	···	$21.0 \pm 1.8 \pm 3.1$	···
$\eta(1760)$	$K^*\bar{K}$	$1.9 \pm 0.4 \pm 0.3$	$-1.53 \pm 0.16 \pm 0.28$	$3.1 \pm 0.4 \pm 0.5$	$-1.16 \pm 0.13 \pm 0.20$
	$a_0\pi$	$2.0 \pm 0.4 \pm 0.3$	$2.11 \pm 0.15 \pm 0.20$	$1.7 \pm 0.4 \pm 0.3$	$3.06 \pm 0.12 \pm 0.24$
	PS	$11.9 \pm 1.8 \pm 2.7$	$1.60 \pm 0.10 \pm 0.19$	$23.2 \pm 2.4 \pm 5.1$	$1.92 \pm 0.07 \pm 0.22$
	Total	$15.8 \pm 1.9 \pm 2.7$	···	$27.9 \pm 2.5 \pm 5.1$	···
$\eta(1405)$	$K^*\bar{K}$	$3.5 \pm 0.6 \pm 1.9$	$-0.10 \pm 0.10 \pm 0.20$	$2.3 \pm 0.5 \pm 0.7$	$-0.01 \pm 0.11 \pm 0.18$
	PS	$5.2 \pm 0.5 \pm 0.8$	$1.77 \pm 0.11 \pm 0.28$	$6.4 \pm 0.5 \pm 0.9$	$1.96 \pm 0.13 \pm 0.20$
	Total	$8.7 \pm 0.8 \pm 2.0$	···	$8.6 \pm 0.7 \pm 1.1$	···
$f_1(1285)$	$a_0\pi$	$2.0 \pm 0.2 \pm 0.2$	$-0.35 \pm 0.13 \pm 0.26$	$2.0 \pm 0.2 \pm 0.2$	$-0.47 \pm 0.11 \pm 0.12$
$f_1(1420)$	$K^*\bar{K}$	$11.4 \pm 0.7 \pm 2.1$	$4.25 \pm 0.08 \pm 0.23$	$6.6 \pm 0.5 \pm 1.7$	$4.67 \pm 0.10 \pm 0.27$
$h_1(1415)$	$K^*\bar{K}[S]$	$10.0 \pm 0.9 \pm 2.0$	$4.59 \pm 0.08 \pm 0.20$	$18.6 \pm 1.2 \pm 3.5$	$1.57 \pm 0.08 \pm 0.55$
	$K^*\bar{K}[D]$	$3.3 \pm 0.3 \pm 0.2$	$-0.13 \pm 0.08 \pm 0.16$	$2.4 \pm 0.3 \pm 0.2$	$-2.57 \pm 0.08 \pm 0.42$
	Total	$13.3 \pm 1.0 \pm 2.0$	···	$21.0 \pm 1.2 \pm 3.6$	···
$f_1(1510)$	$K^*\bar{K}$	$2.9 \pm 0.4 \pm 1.2$	$-3.23 \pm 0.09 \pm 0.47$	$2.6 \pm 0.3 \pm 2.7$	$-2.88 \pm 0.09 \pm 0.23$
$h_1(1595)$	$K^*\bar{K}[S]$	$5.3 \pm 0.8 \pm 1.4$	$1.44 \pm 0.08 \pm 0.19$	$14.8 \pm 1.4 \pm 2.8$	$4.20 \pm 0.06 \pm 0.48$
$\eta_2(1645)$	$K^*\bar{K}$	$1.6 \pm 0.2 \pm 0.8$	$2.28 \pm 0.10 \pm 0.09$	$0.8 \pm 0.2 \pm 0.2$	$2.15 \pm 0.12 \pm 0.09$
PS		$18.2 \pm 2.4 \pm 2.9$	$3.13 \pm 0.09 \pm 0.15$	$25.1 \pm 2.6 \pm 5.0$	$2.85 \pm 0.07 \pm 0.16$
K^*_{ne}		$3.2 \pm 0.4 \pm 0.3$	$-0.87 \pm 0.08 \pm 0.22$	$2.0 \pm 0.3 \pm 0.3$	$-1.36 \pm 0.08 \pm 0.16$
K^*_{ch}		$8.4 \pm 0.7 \pm 0.9$	$-0.86 \pm 0.07 \pm 0.19$	$2.8 \pm 0.4 \pm 1.0$	$-0.82 \pm 0.07 \pm 0.10$
Sum		$118.0 \pm 4.3 \pm 6.2$	···	$135.5 \pm 4.6 \pm 9.7$	···

TABLE VII. Fit fractions and relative-phase differences between the results from amplitude analyses of the $B^+ \to K_S^0 K^- \pi^+ K^+$ and $B^+ \to K_S^0 K^+ \pi^- K^+$ decay modes. The significances $n\sigma_1$ and $n\sigma_2$ defined in the text are also listed for each contribution.

Contribution	Decay	Δf	$n\sigma_1$	$n\sigma_2$	$\Delta\phi$	$n\sigma_1$	$n\sigma_2$
$\eta(1475)$	$K^*\bar{K}$	$0.5 \pm 1.5 \pm 1.8$	0.3	0.2	···	···	···
	$a_0\pi$	$-0.4 \pm 0.6 \pm 0.5$	0.7	0.6	$0.26 \pm 0.24 \pm 0.20$	1.1	0.8
	PS	$6.2 \pm 2.5 \pm 3.5$	2.5	1.5	$-0.24 \pm 0.15 \pm 0.18$	1.6	1.0
	Total	$6.3 \pm 3.0 \pm 3.9$	2.1	1.3	···	···	···
$\eta(1760)$	$K^*\bar{K}$	$-1.1 \pm 0.6 \pm 0.6$	1.9	1.4	$-0.37 \pm 0.21 \pm 0.34$	1.8	0.9
	$a_0\pi$	$0.3 \pm 0.5 \pm 0.4$	0.5	0.4	$-0.95 \pm 0.19 \pm 0.31$	5.0	2.6
	PS	$-11.4 \pm 3.0 \pm 5.8$	3.9	1.8	$-0.32 \pm 0.12 \pm 0.29$	2.6	1.0
	Total	$-12.2 \pm 3.0 \pm 5.8$	4.1	2.0	···	···	···
$\eta(1405)$	$K^*\bar{K}$	$1.2 \pm 0.8 \pm 2.0$	1.5	0.5	$-0.09 \pm 0.15 \pm 0.27$	0.6	0.3
	PS	$-1.2 \pm 0.8 \pm 1.2$	1.5	0.8	$-0.19 \pm 0.17 \pm 0.34$	1.1	0.5
	Total	$0.0 \pm 1.1 \pm 2.3$	0.0	0.0	···	···	···
$f_1(1285)$	$a_0\pi$	$-0.1 \pm 0.3 \pm 0.3$	0.2	0.2	$0.1 \pm 0.2 \pm 0.3$	0.7	0.4
$f_1(1420)$	$K^*\bar{K}$	$4.8 \pm 0.9 \pm 2.7$	5.6	1.7	$-0.4 \pm 0.1 \pm 0.4$	3.3	1.1
$h_1(1415)$	$K^*\bar{K}[S]$	$-8.6 \pm 1.5 \pm 4.1$	5.8	2.0	$3.0 \pm 0.1 \pm 0.6$	26.7	5.1
	$K^*\bar{K}[D]$	$0.9 \pm 0.4 \pm 0.3$	2.4	1.9	$2.4 \pm 0.11 \pm 0.5$	21.6	5.3
	Total	$-7.7 \pm 1.5 \pm 4.1$	5.0	1.8	···	···	···
$f_1(1510)$	$K^*\bar{K}$	$0.3 \pm 0.5 \pm 3.0$	0.6	0.1	$-0.35 \pm 0.13 \pm 0.52$	2.8	0.7
$h_1(1595)$	$K^*\bar{K}[S]$	$-9.5 \pm 1.7 \pm 3.1$	5.8	2.7	$-2.76 \pm 0.10 \pm 0.52$	27.6	5.3
$\eta_2(1645)$	$K^*\bar{K}$	$0.8 \pm 0.3 \pm 0.8$	3.0	0.9	$0.13 \pm 0.16 \pm 0.13$	0.8	0.7
PS		$-6.8 \pm 3.5 \pm 5.8$	2.0	1.0	$0.28 \pm 0.11 \pm 0.22$	2.5	1.1

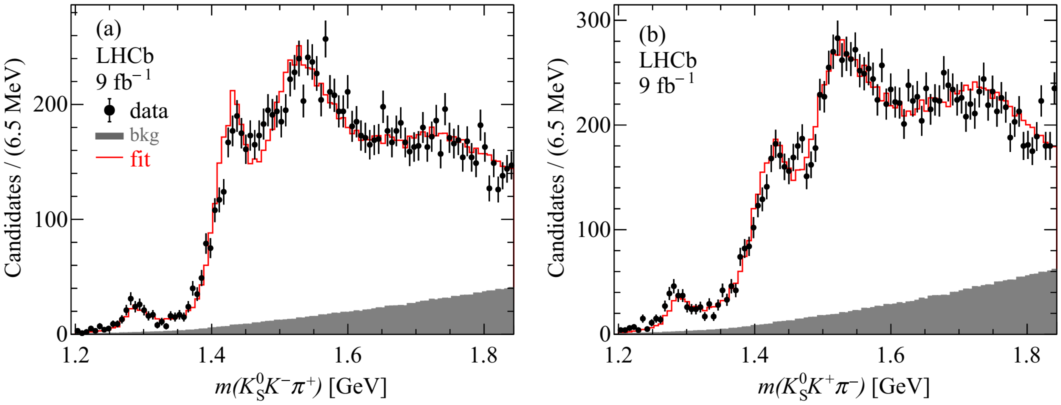

FIG. 15. $K^0_S K\pi$ invariant-mass for (a) $B^+ \to K^0_S K^-\pi^+K^+$ and (b) $B^+ \to K^0_S K^+\pi^-K^+$ candidates with the amplitude analysis fit projections also shown.

when $n\sigma_2$ is considered. In addition it can be noted that relative phases of positive C-parity contributions are consistent, while significant differences are observed for negative C-parity resonance contributions. This effect is observed here for the first time.

In Sec. V a significant difference is found between the $K^0_S K\pi$ Dalitz plots for $B^+ \to K^0_S K^-\pi^+K^+$ and $B^+ \to K^0_S K^+\pi^-K^+$ data which are explained by the observed phase differences in the two decay modes. Figure 15 shows the $K^0_S K\pi$ mass spectrum and Fig. 16 the two-body mass projections for $B^+ \to K^0_S K^-\pi^+K^+$ and $B^+ \to K^0_S K^+\pi^-K^+$ data together with the projections of the fit. Note the different behavior in the $K\pi$ mass distributions between the two decay channels. A reasonable agreement between the fit and the data is observed in all the distributions.

Figures 17 and 18 show the invariant-mass distributions and the fitted functions weighted by Legendre-polynomial moments up to order eight, for $B^+ \to K^0_S K^-\pi^+K^+$ and $B^+ \to K^0_S K^+\pi^-K^+$ data, respectively. A good agreement between the data and the fit is observed for all the

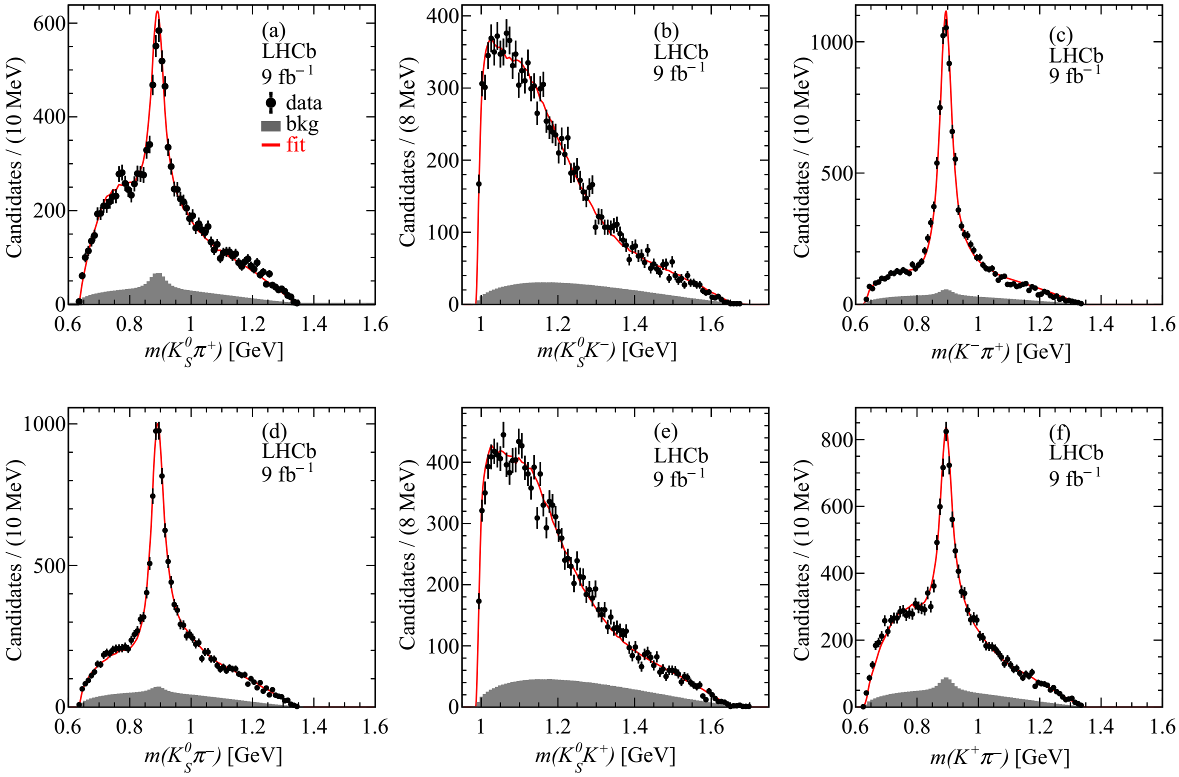

FIG. 16. Two-body invariant-mass distributions for (a)–(c) $B^+ \to K^0_S K^-\pi^+K^+$ and (d)–(f) $B^+ \to K^0_S K^+\pi^-K^+$ candidates with the projections from the amplitude analysis.

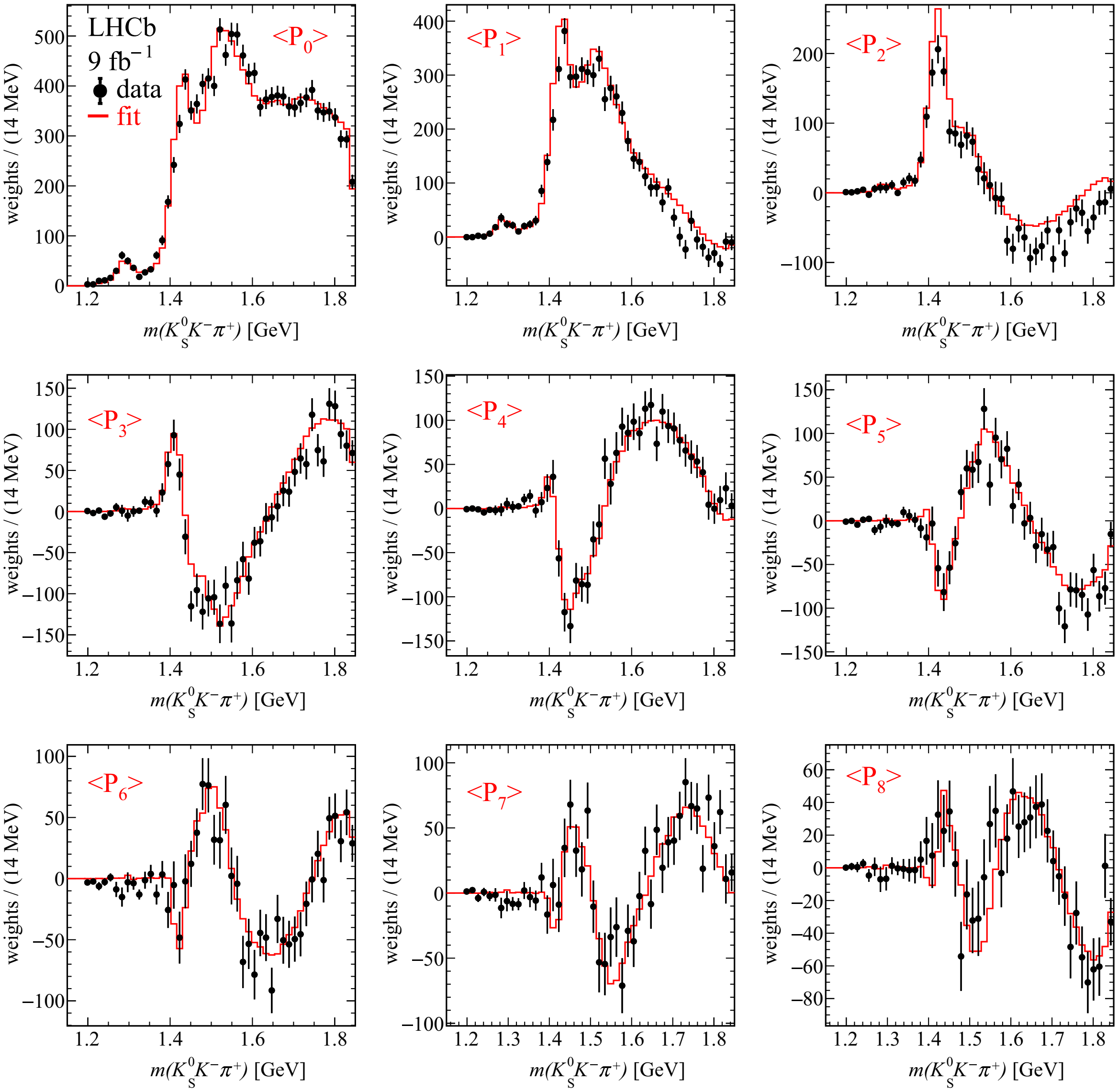

FIG. 17. Fit projections of the $K^0_S K\pi$ mass spectra where both the fit and the data are weighted by Legendre-polynomial moments as functions of $\cos\theta_K$ for $B^+ \to K^0_S K^- \pi^+ K^+$ decays.

distributions, indicating that the fit is capable of reproducing local structure observed in the Dalitz plot. A comparison between the two figures emphasizes once more the difference in the angular distributions between the two B^+ decay modes.

An additional test on the fit quality is performed by evaluating the $\chi^2/\text{n.d.f.}$ value of different two-dimensional distributions, divided into 40×40 cells, following the method described in Sec. V A. The results are listed in Table VIII and confirm the good description of the data in most of the distributions. A few higher $\chi^2/\text{n.d.f.}$ values are present as systematic uncertainties are not included by construction. These are possibly related to imperfections in the fitting model or poor knowledge of the parameters of some resonance contributions [19].

C. Partial-wave decomposition

Figure 19 shows the $K^0_S K\pi$ mass spectra for the two decay modes with contributions of the different resonances superimposed. Here, the squared moduli of the amplitudes are summed over all their partial decay modes.

The composition of the structure around 1.5 GeV resulting from this analysis is rather complex. A superposition of $\eta(1405)$, $f_1(1420)$ and $\eta(1475)$ is present, with similar fractional composition to that obtained from radiative J/ψ decays [11,13]. In addition, significant contributions from $h_1(1415)$, $h_1(1595)$ and $f_1(1510)$ resonances are found. The ratios of fit fractions for the $f_1(1420)$ and $h_1(1415)$ resonances are found to be rather different, $0.86 \pm 0.08 \pm 0.20$ and $0.32 \pm 0.03 \pm 0.10$ for $B^+ \to K^0_S K^- \pi^+ K^+$ and $B^+ \to K^0_S K^+ \pi^- K^+$ decays, respectively [Figs. 19(b) and 19(d)].

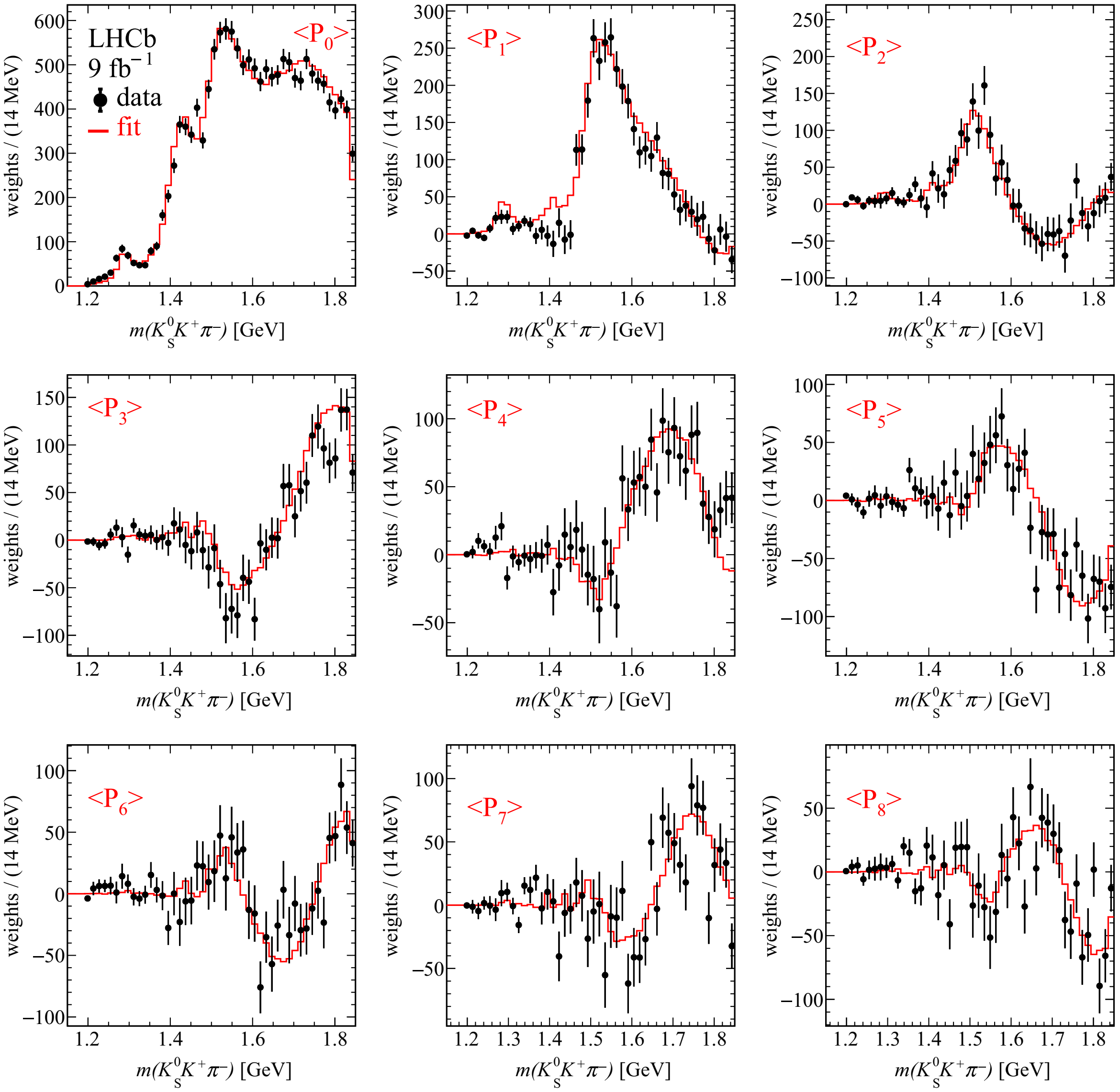

FIG. 18. Fit projections on $K^0_S K\pi$ mass spectra where both the fit and the data are weighted by Legendre-polynomial moments as functions of $\cos\theta_K$ for $B^+ \to K^0_S K^+\pi^- K^+$ decays.

Other experiments also studied the $K^0_S K\pi$ system. The $f_1(1510)$ resonance was first observed in K^-p interactions by the ACNO Collaboration [16] where it is found that this state fits well the hypothesis of being the $s\bar{s}$ member of the $J^{PC} = 1^{++}$ nonet. Furthermore, the $h_1(1415)$ was first observed in K^-p interactions [15] through a significant interference with the $f_1(1510)$ resonance. On the other hand, the $f_1(1420)$ resonance dominates the $K^0_S K\pi$ mass spectrum in central production [14] and a molecular assignment for this resonance has been proposed [17].

VII. SYSTEMATIC UNCERTAINTIES AND TESTS

Several systematic uncertainties are evaluated and listed in Tables XVI and XVII of Appendix B for $B^+ \to K^0_S K^-\pi^+K^+$ and $B^+ \to K^0_S K^+\pi^-K^+$ data, respectively. In the baseline fits the radius r, which enters the Blatt-Weisskopf form factors [42] used by the relativistic BW function describing the $K^*(892)$ resonances, is fixed to 2.5 GeV^{-1} [31]. This value is varied to 1.5 and 3.5 GeV^{-1} and the average of the variations with respect to the baseline fit results is taken as systematic uncertainties (listed as r in Tables XVI and XVII).

The mass and width of the resonances included in this analysis are fixed to their known values, as listed in Table V. Attempts to vary these parameters freely during the fits were unsuccessful due to fit instabilities introduced by the large number of free parameters. The uncertainty associated to this effect is evaluated by performing 100 alternative fits to data where, in each fit, the mass and width of each

TABLE VIII. Results from the χ^2/n.d.f. tests on various two-dimensional distributions for $B^+ \to K^0_S K^- \pi^+ K^+$ and $B^+ \to K^0_S K^+ \pi^- K^+$ data.

B^+ decay mode	Variables	χ^2/n.d.f.
$B^+ \to K^0_S K^- \pi^+ K^+$	$(m(K^0_S K^- \pi^+), \cos\theta_\pi)$	$1328/1113 = 1.19$
	$(m^2(K^- \pi^+), m^2(K^0_S \pi^+))$	$920/809 = 1.14$
	$(m_X(K^- \pi^+), \cos\theta_{K^0})$	$1230/1102 = 1.12$
	$(m_X(K^+ K^- \pi^+), \cos\theta_{K^+})$	$994/964 = 1.03$
	$(m_X(K^0_S \pi^+), \cos\theta_K)$	$1316/1039 = 1.27$
$B^+ \to K^0_S K^+ \pi^- K^+$	$(m(K^0_S K^+ \pi^-), \cos\theta_\pi)$	$1201/1185 = 1.01$
	$(m^2(K^+ \pi^-), m^2(K^0_S \pi^-))$	$1063/847 = 1.25$
	$(m_X(K^+ \pi^-), \cos\theta_{K^0})$	$1222/1142 = 1.07$
	$(m_X(K^+ K^+ \pi^-), \cos\theta_{K^+})$	$1286/1064 = 1.21$
	$(m_X(K^0_S \pi^+), \cos\theta_K)$	$1117/1084 = 1.03$

resonance is randomly sampled from Gaussian functions based on their known values and uncertainties [19], also listed in Table V. The root mean squares of the differences with respect to the baseline fit results are taken as systematic uncertainties (indicated as BW).

The $a_0(980)$ resonance is described by a coupled-channel Breit-Wigner described by Eq. (A3) in Appendix A. The measured parameters describing the resonance are varied within their known statistical uncertainties, and the averages of the absolute deviations from the baseline fit results are taken as systematic uncertainties (indicated as a_0).

The effect of the uncertainty on the efficiency model is evaluated by repeating the fit using a modified model where the last correction term in the functional expressions describing the efficiency in Eq. (7) is removed for both K^0_{SLL} and K^0_{SDD} datasets. The deviations of the fit results from the baseline values are small (indicated as eff).

The uncertainty due to the background model is evaluated by varying within uncertainties the purity of the B^+ signal, listed in Table I, and the fitted fractions of the K^* contributions describing the background model and listed in Table II. The averages of the absolute deviations of the fitted fractions and phases from the baseline fit results are assigned as systematic uncertainties (indicated as bkg).

The $K^0_S K\pi$ mass spectrum has limited phase space near the threshold and a large number of simulation samples are performed to evaluate normalization integrals. To assess the impact on the results, the number of the simulated candidates is doubled and halved and the average of the resulting variations with respect the baseline fit results is taken as systematic uncertainty (indicated as int).

The effect of the trigger (trig) on the composition of the dataset is evaluated by first recomputing separate efficiencies for the two types of trigger samples (described in Sec. II) and separate K^0_{SLL} and K^0_{SDD} simulations. The

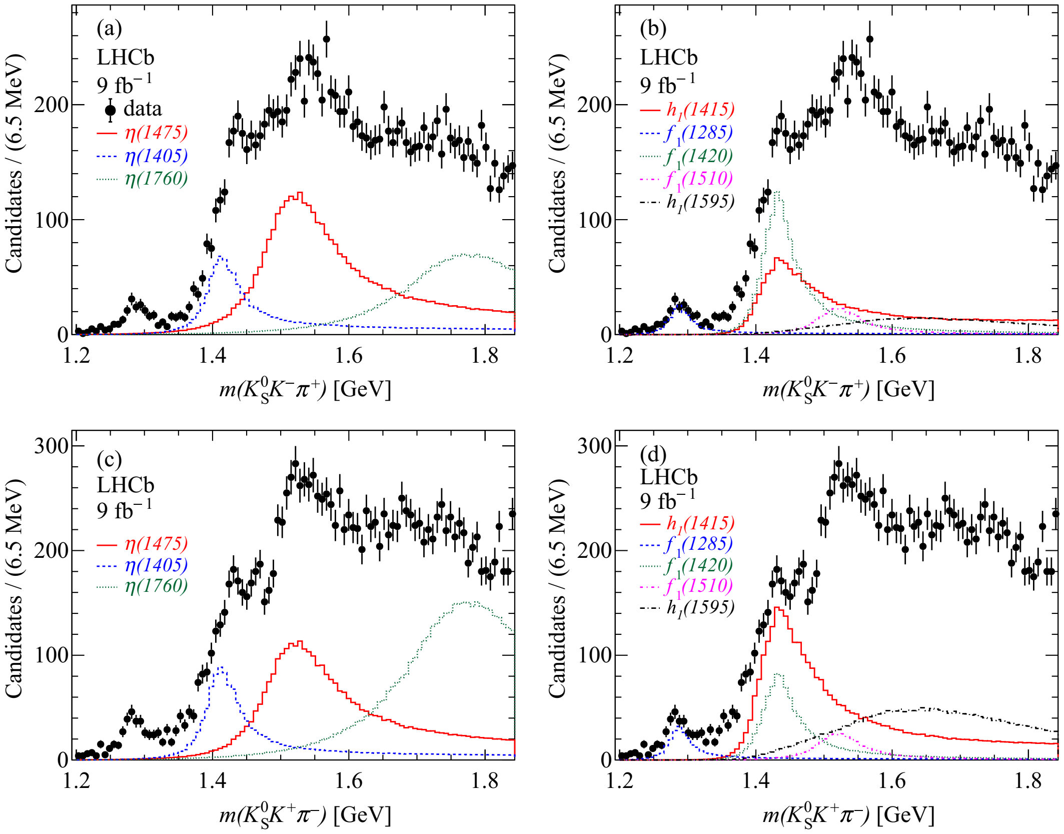

FIG. 19. $K^0_S K\pi$ invariant-mass distribution of (a),(b) $B^+ \to K^0_S K^- \pi^+ K^+$ and (c),(d) $B^+ \to K^0_S K^+ \pi^- K^+$ decays.

$K^0_{\rm S}K^-\pi^+K^+$ and $K^0_{\rm S}K^+\pi^-K^+$ mass spectra are also fitted separately to evaluate the purities in each subsample. Then, the likelihood function given by Eq. (8) is modified in order to include separate contributions for each dataset. The increase of the likelihood value determines a small improvement in the description of the data. The absolute deviations from the baseline fit results are included as systematic uncertainties. The different sources of systematic uncertainties are added in quadrature assuming no correlations among them, with the total uncertainties listed in Tables XVI and XVII in Appendix B.

Further tests of the amplitude model are performed for which no sizable impact on the results is found. Possible fit biases are evaluated by generating, from the baseline fit solution, large samples of pseudoexperiments having the same size as the datasets. These samples are then fitted with the same baseline model, with deviations on the fractions and relative phases from the baseline fit results evaluated. It is found that the average values of these deviations are found to be consistent with zero, and the root-mean-square values of the distributions agree well with the statistical uncertainties resulting from the fits to the data.

The effect of a small discrepancy between data and simulation in the calculation of the tracking efficiency is evaluated by applying corrections to the simulation based on high-yield control samples. It is found that the kinematic variables used in the description of the data and simulation are not affected by these corrections. Charge conjugation on $B^+ \to K^0_{\rm S}K^-\pi^+K^+$ and $B^+ \to K^0_{\rm S}K^+\pi^-K^+$ decays is tested by fitting separately B^+ and B^- data. The differences in the fractions and phases are found consistent with zero within uncertainties.

In Sec. IV [Eq. (5)] it is assumed that the $K^0_{\rm S}K\pi$ system is "decoupled" from the kaon (K_4) which is assumed to be a spectator. This assumption is reasonable given the strong kinematic constraint of $m(K^0_{\rm S}K\pi) < 1.85$ GeV, which removes all possible resonances involving particles from the $K^0_{\rm S}K\pi$ system and the spectator kaon. Therefore two-body and three-body invariant-mass combinations involving the spectator kaon should behave just as phase space (see Appendix C). It is found that the fit reproduces all of the invariant-mass distributions reasonably well.

VIII. MEASUREMENT OF THE BRANCHING FRACTIONS

Branching fractions for the process $B^+ \to R^0K^+$ channels are evaluated. Table IX reports the branching fractions measured in Ref. [31] for $B^+ \to K^0_{\rm S}K^-\pi^+K^+$ and $B^+ \to K^0_{\rm S}K^+\pi^-K^+$ decays using as reference the known $B^+ \to \eta_cK^+$ and $B^+ \to J/\psi K^+$ branching fractions [19].

TABLE IX. Measured branching fractions $\mathcal{B}$ for $B^+ \to K^0_{\rm S}K^-\pi^+K^+$ and $B^+ \to K^0_{\rm S}K^+\pi^-K^+$ from Ref. [31]. The first uncertainty is statistical, the second is systematic and the third is due to the uncertainties on the known $B^+ \to \eta_cK^+$ and $B^+ \to J/\psi K^+$ branching fractions. Inverse-variance-weighted averages of the two measurements are also reported.

Final state	Reference	$\mathcal{B}$ $(\times 10^{-5})$
$B^+ \to K^0K^-\pi^+K^+$	η_c	$32.3 \pm 0.3 \pm 2.0 \pm 7.2$
	J/ψ	$34.0 \pm 0.7 \pm 0.9 \pm 3.1$
	Average	$32.6 \pm 0.3 \pm 0.8 \pm 2.9$
$B^+ \to \bar{K}^0K^+\pi^-K^+$	η_c	$26.6 \pm 0.3 \pm 0.7 \pm 5.9$
	J/ψ	$28.0 \pm 0.7 \pm 1.4 \pm 2.6$
	Average	$26.8 \pm 0.3 \pm 0.6 \pm 2.3$

The amplitude analysis discussed in Sec. VI evaluates the fraction of events f_R for resonance R^0 in the $m(K^0_{\rm S}K\pi) < 1.85$ GeV region. Using this information, it is possible to compute the branching fraction for resonance R^0 as

$$\mathcal{B}(B^+ \to R^0(\to K^0K^\pm\pi^\mp)K^+) = f_R \cdot \mathcal{R} \cdot \mathcal{B} \cdot f_{K^0}, \qquad (13)$$

where f_{K^0} indicates the correction for the unseen K^0 decay modes. This correction takes into account $\mathcal{B}(K^0 \to \pi^+\pi^-) = 0.6920 \pm 0.0005$ [19] and a factor of 2 for the $K^0_{\rm L}$ component in the K^0 meson, yielding a total factor $f_{K^0} = 2.890 \pm 0.001$. The $\mathcal{R}$ factor is computed using efficiency-corrected data as

$$\mathcal{R} = \frac{N(m(K^0_{\rm S}K\pi) < 1.85\ {\rm GeV})}{N_{\rm tot}}, \qquad (14)$$

where $N(m(K^0_{\rm S}K\pi))$ indicates the event yield in the indicated mass region and $N_{\rm tot}$ the total $B \to K^0_{\rm S}K\pi K$ event yield.

To evaluate the above ratios, the total efficiency correction for the four-body decay $B^+ \to K^0_{\rm S}K^-\pi^+K^+$ is used, as described in Ref. [31]. The candidates are weighted by the inverse of the total efficiency, and the resulting $K^0_{\rm S}K\pi K$ mass spectra are fitted to obtain the total B^+ yields. The same method is used to obtain the efficiency-corrected yield for $m(K^0_{\rm S}K\pi) < 1.85$ GeV. Tables X and XI give information on the uncorrected and corrected B^+ yields. Before evaluating the $B^+ \to K^0_{\rm S}K^-\pi^+K^+$ and $B^+ \to K^0_{\rm S}K^+\pi^-K^+$ yields, background contributions from open-charm b-hadron decays $B^+ \to D_{(s)}X$, where X indicates one or two additional particles, must be subtracted.

To account for possible charm resonances in the background, the two- and three-body invariant-mass distributions for B^+ candidates in the mass sideband regions are subtracted from the corresponding distributions of the signal region applying an appropriate normalization. In the mass region $m(K^0_{\rm S}K\pi) < 1.85$ GeV, a $\bar{D}^0 \to K^+\pi^-$ contribution is removed from the $B^+ \to K^0_{\rm S}K^+\pi^-K^+$ candidates, while no open-charm contribution is present for $B^+ \to K^0_{\rm S}K^-\pi^+K^+$ decays.

The resulting ratios are $\mathcal{R} = 0.147 \pm 0.002 \pm 0.003$ for $B^+ \to K^0_{\rm S}K^-\pi^+K^+$ and $\mathcal{R} = 0.206 \pm 0.003 \pm 0.002$ for

TABLE X. Left: uncorrected and right: efficiency-corrected yields of B^+ candidates and charm contributions in $B^+ \to K^0_S K^- \pi^+ K^+$ decays. The second uncertainty in the corrected yields is systematic.

Contribution	Yield	Corrected yield
$B^+ \to K^0_S K^- \pi^+ K^+$	95200 ± 480	$173600 \pm 800 \pm 240$
$D^-_s \to K^0_S K^-$	1490 ± 70	2590 ± 80
$D^0 \to K^+ K^-$	280 ± 30	580 ± 50
$D^0 \to K^0_S K^- K^+$	17130 ± 130	28070 ± 170
$D^0 \to K^0_S K^- \pi^+$	490 ± 40	950 ± 50
Sum of charm	19390 ± 160	32190 ± 200
Charm fraction		$0.180 \pm 0.002 \pm 0.006$
Charmless B^+ decays	78090 ± 430	$142390 \pm 720 \pm 970$
$B^+ \to K^0_S K^- \pi^+ K^+$ $m(K^0_S K \pi) < 1.85$ GeV	11310 ± 150	$20870 \pm 260 \pm 370$

TABLE XI. Left: uncorrected and right: efficiency-corrected yields of B^+ candidates and charm contribution in $B^+ \to K^0_S K^+ \pi^- K^+$ decays. The second uncertainty in the corrected yields is systematic.

Contribution	Yield	Corrected yield
$B^+ \to K^0_S K^+ \pi^- K^+$	68020 ± 120	$131130 \pm 680 \pm 1270$
$D^+_s \to K^0_S K^+$	1090 ± 60	2060 ± 80
$\bar{D}^0 \to K^+ \pi^-$	4460 ± 90	8340 ± 120
$\bar{D}^0 \to K^0_S K^+ \pi^-$	820 ± 40	1660 ± 60
Sum of charm	6370 ± 110	12050 ± 150
Charm fraction		$0.090 \pm 0.002 \pm 0.002$
Charmless B^+ decays	61650 ± 160	$118520 \pm 650 \pm 1170$
$B^+ \to K^0_S K^+ \pi^- K^+$ $m(K^0_S K \pi) < 1.85$ GeV	12600 ± 260	$24770 \pm 280 \pm 20$
$\bar{D}^0 \to K^+ \pi^-$	180 ± 20	410 ± 30
Charm fraction		$0.014 \pm 0.002 \pm 0.002$
Charmless B^+ decays	12420 ± 250	$24410 \pm 280 \pm 60$

$B^+ \to K^0_S K^+ \pi^- K^+$ data. Systematic uncertainties are due to variations of the fit models used for subtraction of the open-charm contributions [31]. The systematic uncertainty on the charm fraction is obtained by comparing results with and without efficiency corrections.

The fractional contributions resulting from the amplitude analysis given in Table VI for $B^+ \to K^0_S K^- \pi^+ K^+$ decays are converted to branching fractions, listed in Table XII. This is achieved by multiplying by the total scaling factor $s = \mathcal{R} \cdot \mathcal{B} \cdot f_{K^0} = (13.84 \pm 0.23 \pm 0.45 \pm 1.19) \times 10^{-5}$, where $\mathcal{B}$ indicates the $B^+ \to K^0_S K^- \pi^+ K^+$ branching

TABLE XII. Measured branching fractions for $B^+ \to R^0 K^+$ from $B^+ \to K^0 K^- \pi^+ K^+$ decays.

Contribution	$\mathcal{B}(B^+ \to R^0 K^+) \times 10^{-5}$
$B^+ \to \eta(1475) K^+ \to (K^* \bar{K}) K^+$	$1.49 \pm 0.15 \pm 0.16 \pm 0.13$
$B^+ \to \eta(1475) K^+ \to (a_0(980)^- \pi^+) K^+$	$0.19 \pm 0.05 \pm 0.05 \pm 0.02$
$B^+ \to \eta(1475) K^+ \to (K^0 K^- \pi^+) K^+$	$2.09 \pm 0.29 \pm 0.31 \pm 0.18$
$B^+ \to \eta(1760) K^+ \to (K^* \bar{K}) K^+$	$0.27 \pm 0.05 \pm 0.05 \pm 0.02$
$B^+ \to \eta(1760) K^+ \to (a_0(980)^- \pi^+) K^+$	$0.28 \pm 0.05 \pm 0.04 \pm 0.02$
$B^+ \to \eta(1760) K^+ \to (K^0 K^- \pi^+) K^+$	$1.64 \pm 0.25 \pm 0.37 \pm 0.14$
$B^+ \to \eta(1405) K^+ \to (K^* \bar{K}) K^+$	$0.48 \pm 0.08 \pm 0.26 \pm 0.04$
$B^+ \to \eta(1405) K^+ \to (K^0 K^- \pi^+) K^+$	$0.72 \pm 0.08 \pm 0.12 \pm 0.06$
$B^+ \to f_1(1285) K^+ \to (a_0(980)^- \pi^+) K^+$	$0.27 \pm 0.03 \pm 0.02 \pm 0.02$
$B^+ \to f_1(1420) K^+ \to (K^* \bar{K}) K^+$	$1.58 \pm 0.10 \pm 0.30 \pm 0.14$
$B^+ \to f_1(1510) K^+ \to (K^* \bar{K}) K^+$	$0.40 \pm 0.05 \pm 0.17 \pm 0.03$
$B^+ \to h_1(1415) K^+ \to (K^* \bar{K}) K^+$	$1.85 \pm 0.14 \pm 0.28 \pm 0.13$
$B^+ \to h_1(1595) K^+ \to (K^* \bar{K}) K^+$	$0.74 \pm 0.12 \pm 0.19 \pm 0.06$
$B^+ \to \eta_2(1645) K^+ \to (K^* \bar{K}) K^+$	$0.22 \pm 0.03 \pm 0.11 \pm 0.02$

TABLE XIII. Measured branching fractions for $B^+ \to R^0 K^+$ from $B^+ \to \bar{K}^0 K^+ \pi^- K^+$ decays.

Contribution	$\mathcal{B}(B^+ \to R^0 K^+) \times 10^{-5}$
$B^+ \to \eta(1475) K^+ \to (K^* \bar{K}) K^+$	$1.42 \pm 0.15 \pm 0.20 \pm 0.12$
$B^+ \to \eta(1475) K^+ \to (a_0(980)^- \pi^+) K^+$	$0.25 \pm 0.06 \pm 0.05 \pm 0.02$
$B^+ \to \eta(1475) K^+ \to (\bar{K}^0 K^+ \pi^-) K^+$	$1.23 \pm 0.20 \pm 0.38 \pm 0.11$
$B^+ \to \eta(1760) K^+ \to (K^* \bar{K}) K^+$	$0.42 \pm 0.06 \pm 0.07 \pm 0.04$
$B^+ \to \eta(1760) K^+ \to (a_0(980)^- \pi^+) K^+$	$0.24 \pm 0.06 \pm 0.04 \pm 0.02$
$B^+ \to \eta(1760) K^+ \to (\bar{K}^0 K^+ \pi^-) K^+$	$3.21 \pm 0.31 \pm 0.71 \pm 0.28$
$B^+ \to \eta(1405) K^+ \to (K^* \bar{K}) K^+$	$0.32 \pm 0.07 \pm 0.09 \pm 0.03$
$B^+ \to \eta(1405) K^+ \to (\bar{K}^0 K^+ \pi^-) K^+$	$0.89 \pm 0.08 \pm 0.13 \pm 0.08$
$B^+ \to f_1(1285) K^+ \to (a_0(980)^- \pi^+) K^+$	$0.28 \pm 0.03 \pm 0.03 \pm 0.02$
$B^+ \to f_1(1420) K^+ \to (K^* \bar{K}) K^+$	$0.92 \pm 0.07 \pm 0.24 \pm 0.08$
$B^+ \to f_1(1510) K^+ \to (K^* \bar{K}) K^+$	$0.36 \pm 0.05 \pm 0.38 \pm 0.03$
$B^+ \to h_1(1415) K^+ \to (K^* \bar{K}) K^+$	$2.91 \pm 0.17 \pm 0.50 \pm 0.22$
$B^+ \to h_1(1595) K^+ \to (K^* \bar{K}) K^+$	$2.05 \pm 0.20 \pm 0.39 \pm 0.18$
$B^+ \to \eta_2(1645) K^+ \to (K^* \bar{K}) K^+$	$0.11 \pm 0.02 \pm 0.03 \pm 0.01$

TABLE XIV. Inverse-variance averages of the branching fraction measurements for $B^+ \to R^0 K^+$ from $B^+ \to K^0 K^- \pi^+ K^+$ and $B^+ \to \bar{K}^0 K^+ \pi^- K^+$ data.

Contribution	$\mathcal{B}(B^+ \to R^0 K^+) \times 10^{-5}$
$B^+ \to \eta(1475) K^+ \to (K^* \bar{K}) K^+$	$1.45 \pm 0.11 \pm 0.12 \pm 0.09$
$B^+ \to \eta(1475) K^+ \to (a_0(980)\pi) K^+$	$0.22 \pm 0.04 \pm 0.03 \pm 0.01$
$B^+ \to \eta(1475) K^+ \to (K^0 K \pi) K^+$	$1.51 \pm 0.16 \pm 0.24 \pm 0.09$
$B^+ \to \eta(1760) K^+ \to (K^* \bar{K}) K^+$	$0.34 \pm 0.04 \pm 0.04 \pm 0.02$
$B^+ \to \eta(1760) K^+ \to (a_0(980)\pi) K^+$	$0.26 \pm 0.04 \pm 0.02 \pm 0.02$
$B^+ \to \eta(1760) K^+ \to (K^0 K \pi) K^+$	$2.21 \pm 0.20 \pm 0.33 \pm 0.13$
$B^+ \to \eta(1405) K^+ \to (K^* \bar{K}) K^+$	$0.38 \pm 0.05 \pm 0.09 \pm 0.02$
$B^+ \to \eta(1405) K^+ \to (K^0 K \pi) K^+$	$0.80 \pm 0.05 \pm 0.09 \pm 0.05$
$B^+ \to f_1(1285) K^+ \to (a_0(980)\pi) K^+$	$0.28 \pm 0.02 \pm 0.02 \pm 0.02$
$B^+ \to f_1(1420) K^+ \to (K^* \bar{K}) K^+$	$1.14 \pm 0.06 \pm 0.19 \pm 0.07$
$B^+ \to f_1(1510) K^+ \to (K^* \bar{K}) K^+$	$0.38 \pm 0.03 \pm 0.15 \pm 0.02$
$B^+ \to h_1(1415) K^+ \to (K^* \bar{K}) K^+$	$2.22 \pm 0.10 \pm 0.23 \pm 0.10$
$B^+ \to h_1(1595) K^+ \to (K^* \bar{K}) K^+$	$1.04 \pm 0.10 \pm 0.12 \pm 0.06$
$B^+ \to \eta_2(1645) K^+ \to (K^* \bar{K}) K^+$	$0.15 \pm 0.02 \pm 0.02 \pm 0.01$

fraction and the third uncertainty is due to the branching fraction $\mathcal{B}$ listed in Table IX.

Similarly, the fractional contributions given in Table VI for $B^+ \to K^0_S K^+ \pi^- K^+$ are converted to branching fractions, listed in Table XIII by multiplying by the total scaling factor $s = \mathcal{R} \cdot \mathcal{B} \cdot f_{K^0} = (15.96 \pm 0.29 \pm 0.43 \pm 1.39) \times 10^{-5}$.

As noted in Sec. VI B the resulting fractions are consistent among the two channels when including the systematic uncertainties. Assuming compatibility between the two sets of measurements, it is possible to evaluate the inverse-variance averages of the two sets of measurements, as given in Table XIV.

IX. SUMMARY

A study is presented of $B^+ \to K^0_S K^- \pi^+ K^+$ and $B^+ \to K^0_S K^+ \pi^- K^+$ decays at proton-proton collision energies of 7, 8 and 13 TeV using the LHCb detector with an integrated luminosity of 9 fb^{-1}. The $K^0_S K \pi$ invariant-mass spectra, in the $m(K^0_S K \pi) < 1.85$ GeV mass region, show a large activity which is resolved using an amplitude analysis. A simple model, where J^{PC} amplitudes are described by multiple Breit-Wigner functions with appropriate angular distributions, provides a good description of the experimental data.

It is found that the $K^0_S K \pi$ mass spectrum is dominated by $J^{PC} = 0^{-+}$, 1^{++} and 1^{-+} amplitudes. Strong interference is observed between the $J^{PC} = 1^{++}$ and $J^{PC} = 1^{-+}$ contributions with different patterns in the two decay modes. Associating the measured amplitudes to known resonances [19], these interference patterns are similar to those observed in $K^- p$ interactions [15] between the $h_1(1415)$ and $f_1(1510)$ resonances. In the present analysis, the contribution from the $f_1(1510)$ is found to be small, with the interference instead generated between the $h_1(1415)$ and $f_1(1420)$ resonances. The presence of two $I = 0$, $J^{PC} = 1^{++}$ resonances that are close in mass, namely the $f_1(1420)$ and $f_1(1510)$, complicates the interpretation as both states compete to be interpreted as the $s\bar{s}$ member of the $J^{PC} = 1^{++}$ nonet [15]. The relative phases of the $J^{PC} = 1^{-+}$ resonances are found to be different in the two final states as a result of the inversion of the population of neutral and charged K^* in the $K^0_S K \pi$ Dalitz plot for $B^+ \to K^0_S K^- \pi^+ K^+$ and $B^+ \to K^0_S K^+ \pi^- K^+$ decays.

A strong $J^{PC} = 0^{-+}$ contribution is found, composed of $\eta(1405)$, $\eta(1475)$ and $\eta(1760)$ resonances. As these states are also observed in J/ψ radiative decays, this suggests that their production mechanisms are possibly similar to those acting in B^+ decays.

The understanding of the $I = 0$, $J^{PC} = 0^{-+}$ nonet is still incomplete, with each of the three η resonances being proposed as candidates for the pseudoscalar glueball [43] (see the review on the spectroscopy of light-meson resonances in Ref. [19]).

In this paper, the first measurements of branching fractions for exclusive $B^+ \to R^0 K^+$ decays are reported, where R^0 is an $I = 0$ resonance having $u\bar{u}$, $s\bar{s}$ or possibly gg content. These results provide new information on light-meson spectroscopy in the low-mass region, offering insights into gluonium physics, a fundamental aspect of QCD. New experimental inputs may arise in the near future from current experiments studying charmonium decays or central production or from future proton-antiproton colliders.

ACKNOWLEDGMENTS

We express our gratitude to our colleagues in the CERN accelerator departments for the excellent performance of the LHC. We thank the technical and administrative staff at the LHCb institutes. We acknowledge support from CERN and from the national agencies: CAPES, CNPq, FAPERJ, and FINEP (Brazil); MOST and NSFC (China); CNRS/IN2P3 (France); BMBF, DFG, and MPG (Germany); INFN (Italy); NWO (Netherlands); MNiSW and NCN (Poland); MCID/IFA (Romania); MICIU and AEI (Spain); SNSF and SER (Switzerland); NASU (Ukraine); STFC (United Kingdom); DOE NP and NSF (USA). We acknowledge the computing resources that are provided by CERN, IN2P3 (France), KIT and DESY (Germany), INFN (Italy), SURF (Netherlands), PIC (Spain), GridPP (United Kingdom), CSCS (Switzerland), IFIN-HH (Romania), CBPF (Brazil), and Polish WLCG (Poland). We are indebted to the communities behind the multiple open-source software packages on which we depend. Individual groups or members have received support from ARC and ARDC (Australia); Key Research Program of Frontier Sciences of CAS, CAS PIFI, CAS CCEPP, Fundamental Research Funds for the Central Universities, and Sci. & Tech. Program of Guangzhou (China); Minciencias (Colombia); EPLANET, Marie Skłodowska-Curie Actions, ERC, and NextGenerationEU

(European Union); A*MIDEX, ANR, IPhU and Labex P2IO, and Région Auvergne-Rhône-Alpes (France); AvH Foundation (Germany); ICSC (Italy); Severo Ochoa and María de Maeztu Units of Excellence, GVA, XuntaGal, GENCAT, InTalent-Inditex and Prog. Atracción Talento CM (Spain); SRC (Sweden); the Leverhulme Trust, the Royal Society, and UKRI (United Kingdom).

DATA AVAILABILITY

The data that support the findings of this article are openly available [44].

APPENDIX A

An amplitude analysis is performed on candidates in the B^+ signal region (see Sec. III) and $m(K^0_S K\pi) < 1.85$ GeV to describe the two B^+ decays and to obtain information on the resonances contributing to the $K^0_S K\pi$ final state. Amplitudes are modeled by the nonrelativistic Zemach-tensor formalism [38–40]. The particles involved in the decay are labeled as

$$B \to \pi_1 K_2 K^0_3 K_4,$$

and the decay is assumed to proceed as

$$B \to R^0 K_4,$$

where R^0 indicates an intermediate resonance which decays as

$$R^0 \to \pi_1 K_2 K^0_3, \tag{A1}$$

and K_4 is assumed to be a spectator. An isobar model is assumed for the decay of the resonance as $R^0 \to Xc$, where X indicates a two-body $X \to ab$ resonance. While the $B \to R^0 K_4$ process is a weak decay and conserves only angular momentum, the $R^0 \to \pi_1 K_2 K^0_3$ transition is a strong decay and conserves angular momentum and parity. In the decay $R^0 \to \pi_1 K_2 K^0_3$, p_i $(i = 1, 2, 3)$ indicate the momenta of the three particles in the rest frame of the $\pi_1 K_2 K^0_3$ system. The amplitudes are defined as follows.

(i) Symmetric and traceless tensors of rank L constructed with p_i are used to describe orbital angular momenta L between the resonance X and c.

(ii) Symmetric and traceless tensors of rank S constructed with t_i are used to describe the spin of the intermediate resonance X. For a resonance X, decaying to the a and b final states, having 3-momenta p_j, p_k with masses m_j and m_k, the t_i are defined as

$$t_i = p_j - p_k - (p_j + p_k)\frac{m_j^2 - m_k^2}{m_{jk}^2}, \tag{A2}$$

with cyclic i, j, k indices.

(iii) The tensors are then combined into a tensor T_J of rank J to obtain the spin J of the $\pi_1 K_2 K^0_3$ system.

(iv) To describe the decay $B \to R^0 K_4$, q_4 indicates the momentum of the kaon K_4 in the B rest frame. A symmetric and traceless tensor Q_J of rank J made with q_4 is used to describe the orbital angular momentum between R^0 and K_4.

(v) Finally, the two T_J and Q_J tensors are contracted to a scalar to obtain the spin of the B meson.

Resonances that can contribute to the decay of the $K^0_S K\pi$ system for $m(K^0_S K\pi) < 1.85$ GeV are $K^*(892)^+$, $K^*(892)^0$, and $a_0(980)$. The $K^*(892)$ resonance is described by a complex spin-1 relativistic BW function with standard Blatt-Weisskopf [42] form factors and a radius r fixed to 2.5 GeV^{-1} [31]. The symbol $K^*(ij)$ in Table XV indicates the $K^*(892)$ BW function formed with the particles combination ij listed in Eq. (A1). The $a_0(980)$ resonance is described by a complex coupled-channel Breit-Wigner function

TABLE XV. Amplitudes used in the Dalitz plot analysis of $B \to (R^0 \to \pi_1 K_2 K^0_3)K_4$ decays, where J^P indicate the R^0 spin parity and L the angular momentum between the subresonance (K^* or a_0) and the other final-state particle. Bold symbols represent three-vectors.

J^P	L	Amplitude (W)
$0^-[S]$	0	$a_0(23)$
$0^-[P]$	1	$K^*(12)(\mathbf{t_3}\cdot\mathbf{p_3}) + GK^*(13)(\mathbf{t_2}\cdot\mathbf{p_2})$
$1^+[S]$	0	$[K^*(12)\mathbf{t_3} + GK^*(13)\mathbf{t_2}]\cdot\mathbf{q_4}$
$1^+[P]$	1	$a_0(23)(\mathbf{p_1}\cdot\mathbf{q_4})$
$1^+[D]$	2	$[K^*(12)\{\mathbf{p_3}(\mathbf{t_3}\cdot\mathbf{p_3}) - \mathbf{\tfrac{1}{3}}(\mathbf{p_3}\cdot\mathbf{p_3})\mathbf{t_3}\} + GK^*(13)\{\mathbf{p_2}(\mathbf{t_2}\cdot\mathbf{p_2}) - \mathbf{\tfrac{1}{3}}(\mathbf{p_2}\cdot\mathbf{p_2})\mathbf{t_2}\}]\cdot\mathbf{q_4}$
1^-	1	$[K^*(12)(\mathbf{t_3}\times\mathbf{p_3}) + GK^*(13)(\mathbf{t_2}\times\mathbf{p_2})]\cdot\mathbf{q_4}$
$2^-[P]$	1	$[K^*(12)\{\frac{1}{2}(t_3^i\cdot p_3^j + t_3^j\cdot p_3^i) - \frac{1}{3}(\mathbf{t_3}\cdot\mathbf{p_3})\delta^{ij}\} + GK^*(13)\{\frac{1}{2}(t_2^i\cdot p_2^j + t_2^j\cdot p_2^i)$ $-\frac{1}{3}(\mathbf{t_2}\cdot\mathbf{p_2})\delta^{ij}\}]\cdot[q_4^i q_4^j - \frac{1}{3}\lvert\mathbf{q_4}\rvert^2\delta^{ij}]$
$2^-[D]$	2	$a_0(23)(p_1^i p_1^j - \frac{1}{3}(\lvert\mathbf{p_1}\rvert^2)\cdot(q_4^i q_4^j - \frac{1}{3}\lvert\mathbf{q_4}\rvert^2\delta^{ij})$
$2^-[F]$	3	$[K^*(12)\{(\mathbf{t_3}\cdot\mathbf{p_3})(p_3^i p_3^j - \frac{1}{3}\lvert\mathbf{p_3}\rvert^2\delta^{ij})\} + GK^*(13)\{(\mathbf{t_2}\cdot\mathbf{p_2})(p_2^i p_2^j - \frac{1}{3}\lvert\mathbf{p_2}\rvert^2\delta^{ij})\}]\cdot[q_4^i q_4^j - \frac{1}{3}\lvert\mathbf{q_4}\rvert^2\delta^{ij}]$
2^+	2	$[K^*(12)\{\frac{1}{2}(\mathbf{t_3}\times\mathbf{p_3})^i p_3^j + p_3^i(\mathbf{t_3}\times\mathbf{p_3})^j\} - \frac{1}{3}\{(\mathbf{t_3}\times\mathbf{p_3})\cdot\mathbf{p_3}\}\delta^{ij}$ $+GK^*(13)\{\frac{1}{2}[\mathbf{t_2}\times\mathbf{p_2})^i p_2^j + p_2^i(\mathbf{t_2}\times\mathbf{p_2})^j\} - \frac{1}{3}\{(\mathbf{t_2}\times\mathbf{p_2})\cdot\mathbf{p_2}\}\delta^{ij}]\cdot[q_4^i q_4^j - \frac{1}{3}\lvert\mathbf{q_4}\rvert^2\delta^{ij}]$

$$a_0(m) = \frac{g_2}{m_0^2 - m^2 - i(\rho_1 g_1^2 + \rho_2 g_2^2)}, \qquad \text{(A3)}$$

where ρ_1 and ρ_2 and g_1 and g_2 are phase-space factors and couplings, respectively, to the $\eta\pi$ (1) and $K\bar{K}$ (2) final states. The $a_0(980)$ parameters are fixed to the values $m_0 = 999 \pm 2$ MeV, $g_1 = 324 \pm 15$ MeV, and $g_2^2/g_1^2 = 1.03 \pm 0.14$ [45] and the corresponding BW function is indicated with $a_0(23)$ in Table XV.

For isospin $I = 0$ resonances, the interference between neutral $K^*(12)$ and charged $K^*(13)$ is fixed by G parity, being constructive for $G = +1$ and destructive for $G = -1$. Note, however, that as G parity is related to C parity by $G = C(-1)^I$, an additional minus sign is added to the above definitions of the 3-momenta to ensure correct transformation under C parity instead, such that constructive interference is obtained with $G = -1$ and vice versa.

Table XV lists the amplitudes used in this analysis. Asymmetries between the charged and neutral K^* can be generated by interference between $I = 0$ amplitudes having opposite C parities or by interfering $I = 0$ and $I = 1$ amplitudes. In this analysis, no evidence is found of contributing $I = 1$ amplitudes.

In the $B \to R^0 K_4$ decay, R^0 resonances are described with the BW function given in Eq. (12) multiplied by the appropriate spin-parity terms $W(\vec{x})$ described in Table XV.

APPENDIX B

Systematic uncertainties on the measured fit fractions and phases are listed in Tables XVI and XVII.

TABLE XVI. Absolute systematic uncertainties on fractions and phases for the $B^+ \to K_S^0 K^- \pi^+ K^+$ decay.

		Fractions [%]							
Contribution	Decay mode	r	BW	a_0	Efficiency	Background	Integrals	Trigger	Total
$\eta(1475)$	$K^*\bar{K}$	0.07	1.04	0.05	0.07	0.02	0.28	0.02	1.08
	$a_0\pi$	0.10	0.30	0.08	0.04	0.04	0.02	0.17	0.37
	PS	0.26	1.99	0.30	0.57	0.08	0.16	0.22	2.13
$\eta(1760)$	$K^*\bar{K}$	0.02	0.31	0.01	0.01	0.02	0.06	0.01	0.32
	$a_0\pi$	0.08	0.19	0.05	0.04	0.03	0.01	0.21	0.30
	PS	0.42	2.60	0.09	0.05	0.11	0.26	0.05	2.65
$\eta(1405)$	$K^*\bar{K}$	0.03	1.86	0.04	0.14	0.02	0.08	0.03	1.87
	PS	0.03	0.80	< 0.01	0.09	0.02	0.02	0.06	0.81
$f_1(1285)$	$a_0\pi$	< 0.01	0.14	0.01	0.04	< 0.01	0.04	0.03	0.15
$f_1(1420)$	$K^*\bar{K}$	0.06	2.10	0.03	0.23	0.02	0.13	0.32	2.14
$h_1(1415)$	$K^*\bar{K}[S]$	0.06	1.86	0.01	0.16	0.02	0.19	0.56	1.96
	$K^*\bar{K}[D]$	0.04	0.11	< 0.01	0.11	< 0.01	0.09	0.08	0.20
$f_1(1510)$	$K^*\bar{K}$	< 0.01	1.18	0.01	0.10	0.01	0.06	0.03	1.19
$h_1(1595)$	$K^*\bar{K}[S]$	0.09	0.82	0.02	0.19	0.23	0.19	1.02	1.36
$\eta_2(1645)$	$K^*\bar{K}$	0.03	0.80	< 0.01	0.08	< 0.01	0.02	0.07	0.81
PS		0.82	2.71	0.04	0.17	0.10	0.28	0.42	2.88
K^*_{ne}		0.11	0.19	0.01	0.03	0.02	0.07	0.11	0.26
K^*_{ch}		0.16	0.80	0.02	0.19	0.04	0.25	0.26	0.91

		Phases [rad]							
Contribution	Decay mode	r	BW	a_0	Eff	Bkg	Int	Trig	Total
$\eta(1475)$	$a_0\pi$	0.01	0.09	0.04	0.01	0.01	0.04	0.11	0.16
	PS	0.01	0.10	0.01	0.03	0.01	<0.01	0.06	0.12
$\eta(1760)$	$K^*\bar{K}$	<0.01	0.20	0.01	0.16	0.09	0.02	0.06	0.28
	$a_0\pi$	0.01	0.16	0.04	0.10	0.01	0.01	0.03	0.21
	PS	0.01	0.19	0.01	0.02	<0.01	0.01	0.01	0.20
$\eta(1405)$	$K^*\bar{K}$	0.02	0.13	<0.01	0.14	<0.01	0.02	0.03	0.20
	PS	<0.01	0.19	<0.01	0.19	<0.01	0.01	0.08	0.31
$f_1(1285)$	$a_0\pi$	0.01	0.24	0.04	0.05	0.01	<0.01	0.08	0.26
$f_1(1420)$	$K^*\bar{K}$	<0.01	0.22	<0.01	0.05	<0.01	0.02	0.05	0.23
$h_1(1415)$	$K^*\bar{K}[S]$	0.01	0.18	<0.01	0.05	<0.01	0.02	0.06	0.20
	$K^*\bar{K}[D]$	<0.01	0.07	<0.01	0.14	<0.01	0.01	0.05	0.16
$f_1(1510)$	$K^*\bar{K}$	<0.01	0.20	<0.01	0.42	<0.01	0.02	0.09	0.48

(Table continued)

TABLE XVI. *(Continued)*

		Fractions [%]							
Contribution	Decay mode	r	BW	a_0	Efficiency	Background	Integrals	Trigger	Total
$h_1(1595)$	$K^*\bar{K}[S]$	<0.01	0.16	<0.01	0.10	<0.01	0.01	<0.01	0.19
$\eta_2(1645)$	$K^*\bar{K}$	0.01	0.07	<0.01	<0.01	<0.01	<0.01	0.05	0.09
PS		0.01	0.14	<0.01	0.03	< 0.01	0.01	0.04	0.15
K^*_{ne}		0.01	0.08	<0.01	0.19	< 0.01	0.02	0.06	0.22
K^*_{ch}		<0.01	0.06	<0.01	0.18	< 0.01	0.01	0.01	0.19

TABLE XVII. Absolute systematic uncertainties on fractions and phases for the $B^+ \to K^0_S K^+ \pi^- K^+$ decay.

		Fractions [%]							
Contribution	Decay mode	r	BW	a_0	Eff	Bkg	Int	Trig	Total
$\eta(1475)$	$K^*\bar{K}$	0.13	1.28	0.11	0.09	0.03	0.07	0.59	1.43
	$a_0\pi$	0.14	0.30	0.11	0.04	0.02	0.08	0.01	0.62
	PS	0.12	2.23	1.17	0.31	0.07	0.08	1.03	2.74
$\eta(1760)$	$K^*\bar{K}$	0.09	0.40	0.19	0.02	0.01	0.02	0.07	0.53
	$a_0\pi$	0.07	0.23	0.11	0.03	0.01	0.03	0.08	0.29
	PS	0.48	4.57	2.04	0.09	0.08	0.55	0.77	6.15
$\eta(1405)$	$K^*\bar{K}$	0.08	0.57	0.22	0.08	0.01	0.03	0.23	0.73
	PS	0.17	0.77	0.19	0.10	0.01	0.05	0.41	3.54
$f_1(1285)$	$a_0\pi$	0.01	0.19	0.02	0.05	<0.01	0.03	0.14	0.54
$f_1(1420)$	$K^*\bar{K}$	0.01	1.49	0.80	0.09	0.01	0.12	0.01	1.71
$h_1(1415)$	$K^*\bar{K}[S]$	0.14	3.19	1.47	0.25	0.02	0.27	0.16	3.54
	$K^*\bar{K}[D]$	0.01	0.11	0.16	0.09	0.01	0.03	0.09	0.24
$f_1(1510)$	$K^*\bar{K}$	0.08	2.72	0.06	0.10	<0.01	0.07	0.26	2.74
$h_1(1595)$	$K^*\bar{K}[S]$	0.08	2.17	1.64	0.44	0.03	0.16	0.09	2.77
$\eta_2(1645)$	$K^*\bar{K}$	0.02	0.05	0.13	0.05	<0.01	0.02	0.10	0.18
PS		0.81	4.79	1.19	0.07	0.07	0.42	0.26	7.33
K^*_{ne}		0.06	0.25	0.19	0.03	0.03	0.01	0.05	0.37
K^*_{ch}		0.09	0.21	0.94	0.08	0.04	0.07	0.08	0.97

		Phases [rad]							
Contribution	Decay mode	r	BW	a_0	Eff	Bkg	Int	Trig	Total
$\eta(1475)$	$a_0\pi$	0.02	0.11	0.07	<0.01	0.01	0.02	0.01	0.13
	PS	0.01	0.12	0.05	<0.01	<0.01	0.02	<0.01	0.14
$\eta(1760)$	$K^*\bar{K}$	0.01	0.19	0.07	0.01	<0.01	0.02	0.01	0.21
	$a_0\pi$	0.01	0.13	0.19	0.01	0.01	0.02	0.07	0.25
	PS	0.01	0.20	0.06	<0.01	<0.01	0.01	0.06	0.22
$\eta(1405)$	$K^*\bar{K}$	0.02	0.18	0.02	<0.01	<0.01	0.02	0.01	0.18
	PS	0.02	0.19	0.03	<0.01	0.01	0.01	0.06	0.20
$f_1(1285)$	$a_0\pi$	0.01	0.09	0.04	0.01	0.01	0.01	0.07	0.14
$f_1(1420)$	$K^*\bar{K}$	0.02	0.26	0.07	<0.01	<0.01	0.02	0.02	0.27
$h_1(1415)$	$K^*\bar{K}[S]$	0.01	0.19	0.51	<0.01	<0.01	0.01	0.03	0.55
	$K^*\bar{K}[D]$	0.01	0.08	0.41	<0.01	<0.01	0.03	0.06	0.42
$f_1(1510)$	$K^*\bar{K}$	<0.01	0.19	0.06	0.02	<0.01	0.02	0.12	0.24
$h_1(1595)$	$K^*\bar{K}[S]$	0.01	0.15	0.46	0.01	<0.01	0.01	0.01	0.48
$\eta_2(1645)$	$K^*\bar{K}$	0.01	0.07	0.02	0.03	<0.01	0.03	0.01	0.09
PS		0.11	0.11	0.05	0.01	<0.01	0.01	0.01	0.17
K^*_{ne}		0.07	0.07	0.08	<0.01	<0.01	0.01	0.10	0.16
K^*_{ch}		0.07	0.07	0.01	0.01	<0.01	0.02	0.02	0.10

APPENDIX C

Figures 20 and 21 show the mass distributions of two- and three-body final-state particles involving the spectator kaon for $B^+ \to K^0_S K^- \pi^+ K^+$ and $B^+ \to K^0_S K^+ \pi^- K^+$ data. The agreement between the fit and data is reasonable with all distributions and fit projections being consistent with phase space, as expected.

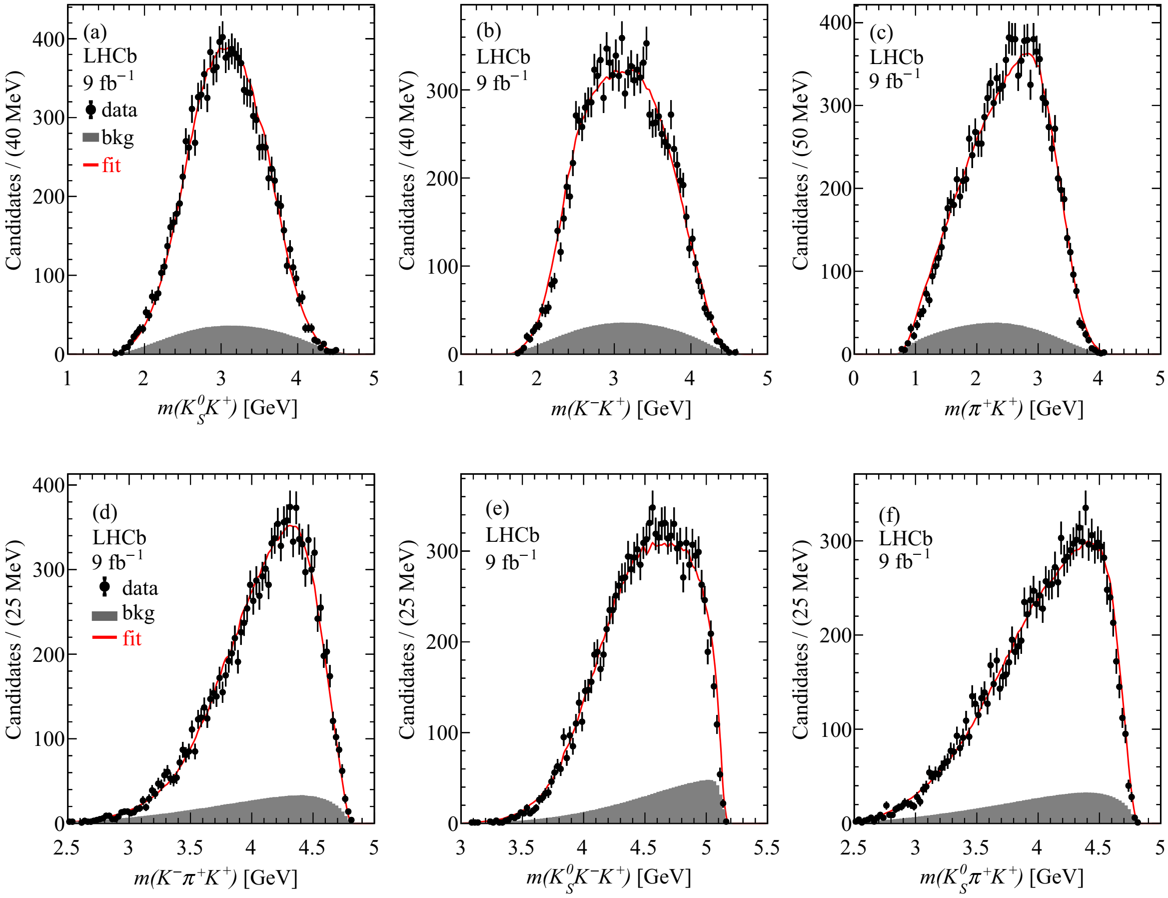

FIG. 20. Invariant-mass distributions and fit projections of (a)–(c) two- and (d)–(f) three-body final-state particles involving the spectator kaon for $B^+ \to K^0_S K^- \pi^+ K^+$ data.

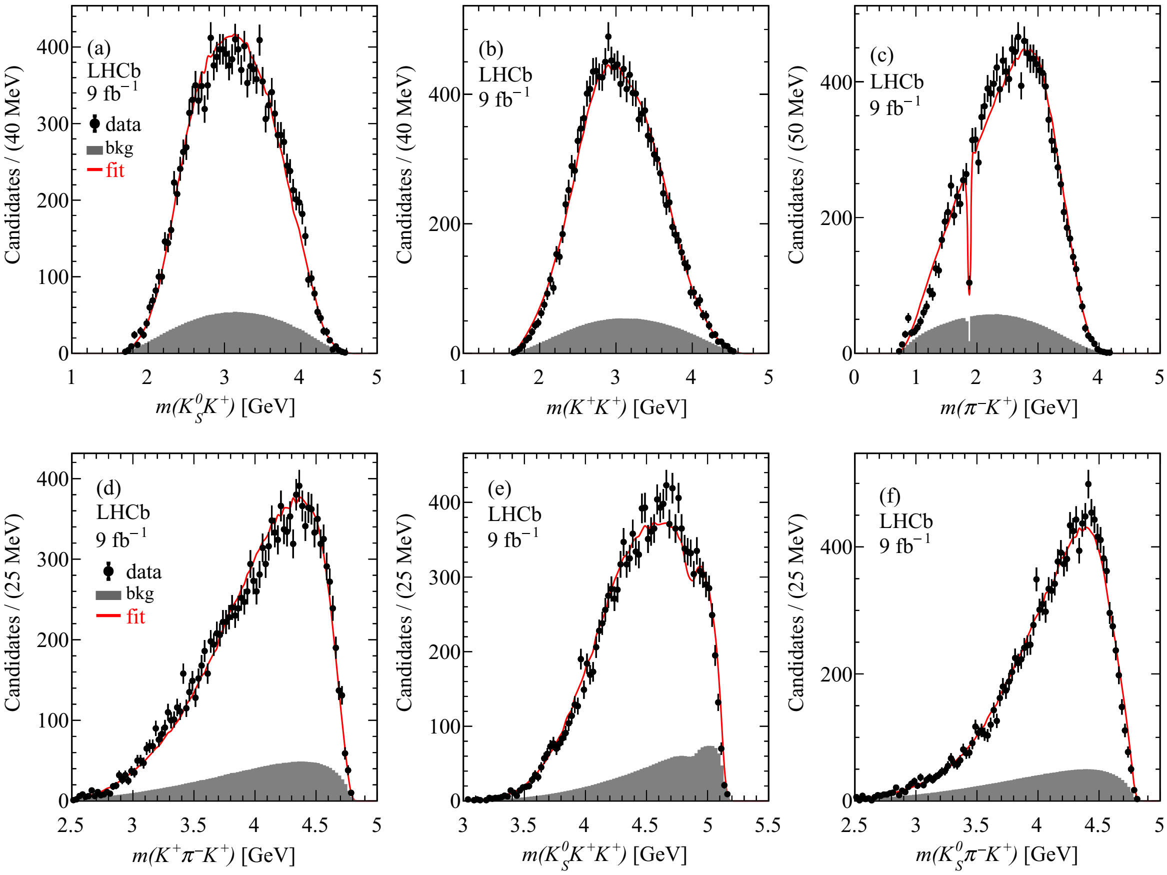

FIG. 21. Invariant-mass distribution of (a)–(c) two- and (d)–(f) three-body final-state particles involving the spectator kaon for $B^+ \to K^0_S K^+\pi^-K^+$ data. The depletion in (c) is due to the removal of the open-charm contribution due to $\bar{D}^0 \to K^+\pi^-$ decays.

---

[1] E. Klempt and A. Zaitsev, Glueballs, hybrids, multiquarks. Experimental facts versus QCD inspired concepts, Phys. Rep. **454**, 1 (2007).

[2] Y. Chen *et al.*, Glueball spectrum and matrix elements on anisotropic lattices, Phys. Rev. D **73**, 014516 (2006).

[3] W. Ochs, The status of glueballs, J. Phys. G **40**, 043001 (2013).

[4] H.-X. Chen, W. Chen, X. Liu, Y.-R. Liu, and S.-L. Zhu, An updated review of the new hadron states, Rep. Prog. Phys. **86**, 026201 (2023).

[5] R. L. Jaffe and K. Johnson, Unconventional states of confined quarks and gluons, Phys. Lett. **60B**, 201 (1976).

[6] C. E. Carlson, T. H. Hansson, and C. Peterson, Meson, baryon and glueball masses in the MIT bag model, Phys. Rev. D **27**, 1556 (1983); **28**, 2985(E) (1983).

[7] M. S. Chanowitz and S. R. Sharpe, Hybrids: Mixed states of "quarks and gluons", Nucl. Phys. **B222**, 211 (1983); **B228**, 588(E) (1983).

[8] D. L. Scharre *et al.* (Mark-II Collaboration), Observation of the radiative transition $\psi \to \gamma E(1420)$, Phys. Lett. **97B**, 329 (1980).

[9] C. Edwards *et al.* (Crystal-Ball Collaboration), Observation of a pseudoscalar state at 1440 MeV in J/ψ radiative decays, Phys. Rev. Lett. **49**, 259 (1982); **50**, 219(E) (1983).

[10] L. Kopke and N. Wermes, J/ψ decays, Phys. Rep. **174**, 67 (1989).

[11] Z. Bai *et al.* (MARK-III Collaboration), Partial wave analysis of $J/\psi \to \gamma K^0_S K^\pm \pi^\mp$, Phys. Rev. Lett. **65**, 2507 (1990).

[12] M. Ablikim *et al.* (BES Collaboration), Pseudoscalar production at $\omega\omega$ threshold in $J/\psi \to \gamma\omega\omega$, Phys. Rev. D **73**, 112007 (2006).

[13] M. Ablikim *et al.* (BESIII Collaboration), Study of $\eta(1405)/\eta(1475)$ in $J/\psi \to \gamma K^0_S K^0_S \pi^0$ decay, J. High Energy Phys. 03 (2023) 121.

[14] T. A. Armstrong *et al.* (WA76 Collaboration), Study of the centrally produced $K_1^0 K^\pm \pi^\mp$ system at 85 GeV/c, Z. Phys. C **34**, 23 (1987).

[15] D. Aston *et al.*, Evidence for two strangeonium resonances with $J^{PC} = 1^{++}$ and 1^{+-} in $K^- p$ interactions at 11 GeV/c, Phys. Lett. B **201**, 573 (1988).

[16] P. Gavillet, R. Armenteros, M. Aguilar-Benítez, M. Mazzucato, and C. Dionisi, Evidence for a new $K^* \bar{K}$ state at a mass of 1530 MeV with $IJ^{(PC)} = 01^{++}$ observed in $K^- p$ interactions at 4.2 GeV/c, Z. Phys. C **16**, 119 (1982).

[17] R. S. Longacre, The $E(1420)$ meson as a $K\bar{K}\pi$ molecule, Phys. Rev. D **42**, 874 (1990).

[18] H. Fritzsch, The gluonic decay of the b-quark and the η'-meson, Phys. Lett. B **415**, 83 (1997).

[19] S. Navas *et al.* (Particle Data Group), Review of particle physics, Phys. Rev. D **110**, 030001 (2024).

[20] B. Aubert *et al.* (*BABAR* Collaboration), Study of B meson decays with excited η and η' mesons, Phys. Rev. Lett. **101**, 091801 (2008).

[21] A. A. Alves, Jr. *et al.* (LHCb Collaboration), The LHCb detector at the LHC, J. Instrum. **3**, S08005 (2008).

[22] LHCb Collaboration, LHCb detector performance, Int. J. Mod. Phys. A **30**, 1530022 (2015).

[23] R. Aaij *et al.*, Performance of the LHCb vertex locator, J. Instrum. **9**, P09007 (2014).

[24] R. Aaij *et al.*, The LHCb trigger and its performance in 2011, J. Instrum. **8**, P04022 (2013).

[25] T. Sjöstrand, S. Mrenna, and P. Skands, A brief introduction to PYTHIA 8.1, Comput. Phys. Commun. **178**, 852 (2008); PYTHIA 6.4 physics and manual, J. High Energy Phys. 05 (2006) 026.

[26] I. Belyaev *et al.*, Handling of the generation of primary events in Gauss, the LHCb simulation framework, J. Phys. Conf. Ser. **331**, 032047 (2011).

[27] D. J. Lange, The EvtGen particle decay simulation package, Nucl. Instrum. Methods Phys. Res., Sect. A **462**, 152 (2001).

[28] N. Davidson, T. Przedzinski, and Z. Was, PHOTOS interface in C++: Technical and physics documentation, Comput. Phys. Commun. **199**, 86 (2016).

[29] J. Allison *et al.* (Geant4 Collaboration), Geant4 developments and applications, IEEE Trans. Nucl. Sci. **53**, 270 (2006); S. Agostinelli *et al.* (Geant4 Collaboration), Geant4: A simulation toolkit, Nucl. Instrum. Methods Phys. Res., Sect. A **506**, 250 (2003).

[30] M. Clemencic, G. Corti, S. Easo, C. R. Jones, S. Miglioranzi, M. Pappagallo, and P. Robbe, The LHCb simulation application, Gauss: Design, evolution and experience, J. Phys. Conf. Ser. **331**, 032023 (2011).

[31] R. Aaij *et al.* (LHCb Collaboration), Study of charmonium decays to $K_S^0 K\pi$ in the $B \to (K_S^0 K\pi)K$ channels, Phys. Rev. D **108**, 032010 (2023).

[32] W. D. Hulsbergen, Decay chain fitting with a Kalman filter, Nucl. Instrum. Methods Phys. Res., Sect. A **552**, 566 (2005).

[33] L. Breiman, J. H. Friedman, R. A. Olshen, and C. J. Stone, *Classification and Regression Trees* (Wadsworth International Group, Belmont, California, USA, 1984).

[34] Y. Freund and R. E. Schapire, A decision-theoretic generalization of on-line learning and an application to boosting, J. Comput. Syst. Sci. **55**, 119 (1997).

[35] H. Voss, A. Hoecker, J. Stelzer, and F. Tegenfeldt, TMVA—Toolkit for multivariate data analysis with ROOT, Proc. Sci. ACAT2007 (**2007**) 040; A. Hoecker *et al.*, TMVA 4—Toolkit for multivariate data analysis with ROOT. Users guide, arXiv:physics/0703039.

[36] B. P. Roe, H.-J. Yang, J. Zhu, Y. Liu, I. Stancu, and G. McGregor, Boosted decision trees, an alternative to artificial neural networks, Nucl. Instrum. Methods Phys. Res., Sect. A **543**, 577 (2005).

[37] R. Aaij *et al.* (LHCb Collaboration), Amplitude analysis of $B_s^0 \to K_S^0 K^\pm \pi^\mp$ decays, J. High Energy Phys. 06 (2019) 114.

[38] C. Zemach, Three pion decays of unstable particles, Phys. Rev. **133**, B1201 (1964).

[39] C. Dionisi *et al.*, Observation and quantum numbers determination of the E(1420) meson in $\pi^- p$ interactions at 3.95 GeV/c, Nucl. Phys. **B169**, 1 (1980).

[40] V. Filippini, A. Fontana, and A. Rotondi, Covariant spin tensors in meson spectroscopy, Phys. Rev. D **51**, 2247 (1995).

[41] F. James, Monte-Carlo phase space, CERN Program Library (1968).

[42] J. M. Blatt and V. F. Weisskopf, *Theoretical Nuclear Physics* (Springer, New York, 1952).

[43] H.-n. Li, Dispersive analysis of glueball masses, Phys. Rev. D **104**, 114017 (2021).

[44] Data associated to the plots in this publication as well as in supplementary materials are available at https://cds.cern.ch/record/2921538/files.

[45] A. Abele *et al.* (Crystal Barrel Collaboration), $p\bar{p}$ annihilation at rest into $K_L K^\pm \pi^\mp$, Phys. Rev. D **57**, 3860 (1998).

R. Aaij,[38] A. S. W. Abdelmotteleb,[57] C. Abellan Beteta,[51] F. Abudinén,[57] T. Ackernley,[61] A. A. Adefisoye,[69]
B. Adeva,[47] M. Adinolfi,[55] P. Adlarson,[82] C. Agapopoulou,[14] C. A. Aidala,[83] Z. Ajaltouni,[11] S. Akar,[11]
K. Akiba,[38] P. Albicocco,[28] J. Albrecht,[19,b] F. Alessio,[49] M. Alexander,[60] Z. Aliouche,[63] P. Alvarez Cartelle,[56]
R. Amalric,[16] S. Amato,[3] J. L. Amey,[55] Y. Amhis,[14] L. An,[6] L. Anderlini,[27] M. Andersson,[51]
A. Andreianov,[44] P. Andreola,[51] M. Andreotti,[26] D. Andreou,[69] A. Anelli,[31,49,c] D. Ao,[7] F. Archilli,[37,d]
M. Argenton,[26] S. Arguedas Cuendis,[9,49] A. Artamonov,[44] M. Artuso,[69] E. Aslanides,[13] R. Ataíde Da Silva,[50]
M. Atzeni,[65] B. Audurier,[12] D. Bacher,[64] I. Bachiller Perea,[10] S. Bachmann,[22] M. Bachmayer,[50] J. J. Back,[57]
P. Baladron Rodriguez,[47] V. Balagura,[15] A. Balboni,[26] W. Baldini,[26] L. Balzani,[19] H. Bao,[7]

J. Baptista de Souza Leite,[61] C. Barbero Pretel,[47,12] M. Barbetti,[27] I. R. Barbosa,[70] R. J. Barlow,[63]
M. Barnyakov,[25] S. Barsuk,[14] W. Barter,[59] J. Bartz,[69] J. M. Basels,[17] S. Bashir,[40] G. Bassi,[35,e] B. Batsukh,[5]
P. B. Battista,[14] A. Bay,[50] A. Beck,[57] M. Becker,[19] F. Bedeschi,[35] I. B. Bediaga,[2] N. A. Behling,[19] S. Belin,[47]
K. Belous,[44] I. Belov,[29] I. Belyaev,[36] G. Benane,[13] G. Bencivenni,[28] E. Ben-Haim,[16] A. Berezhnoy,[44]
R. Bernet,[51] S. Bernet Andres,[45] A. Bertolin,[33] C. Betancourt,[51] F. Betti,[59] J. Bex,[56] Ia. Bezshyiko,[51]
J. Bhom,[41] M. S. Bieker,[19] N. V. Biesuz,[26] P. Billoir,[16] A. Biolchini,[38] M. Birch,[62] F. C. R. Bishop,[10]
A. Bitadze,[63] A. Bizzeti, T. Blake,[57] F. Blanc,[50] J. E. Blank,[19] S. Blusk,[69] V. Bocharnikov,[44]
J. A. Boelhauve,[19] O. Boente Garcia,[15] T. Boettcher,[66] A. Bohare,[59] A. Boldyrev,[44] C. S. Bolognani,[79]
R. Bolzonella,[26,f] R. B. Bonacci,[1] N. Bondar,[44] A. Bordelius,[49] F. Borgato,[33,g] S. Borghi,[63] M. Borsato,[31,c]
J. T. Borsuk,[41] E. Bottalico,[61] S. A. Bouchiba,[50] M. Bovill,[64] T. J. V. Bowcock,[61] A. Boyer,[49] C. Bozzi,[26]
J. D. Brandenburg,[84] A. Brea Rodriguez,[50] N. Breer,[19] J. Brodzicka,[41] A. Brossa Gonzalo,[47,a] J. Brown,[61]
D. Brundu,[32] E. Buchanan,[59] L. Buonincontri,[33,g] M. Burgos Marcos,[79] A. T. Burke,[63] C. Burr,[49] J. S. Butter,[56]
J. Buytaert,[49] W. Byczynski,[49] S. Cadeddu,[32] H. Cai,[74] A. Caillet,[16] R. Calabrese,[26,f] S. Calderon Ramirez,[9]
L. Calefice,[46] S. Cali,[28] M. Calvi,[31,c] M. Calvo Gomez,[45] P. Camargo Magalhaes,[2,h] J. I. Cambon Bouzas,[47]
P. Campana,[28] D. H. Campora Perez,[79] A. F. Campoverde Quezada,[7] S. Capelli,[31] L. Capriotti,[26]
R. Caravaca-Mora,[9] A. Carbone,[25,i] L. Carcedo Salgado,[47] R. Cardinale,[29,j] A. Cardini,[32] P. Carniti,[31,c]
L. Carus,[22] A. Casais Vidal,[65] R. Caspary,[22] G. Casse,[61] M. Cattaneo,[49] G. Cavallero,[26,49] V. Cavallini,[26,f]
S. Celani,[22] S. Cesare,[30,k] A. J. Chadwick,[61] I. Chahrour,[83] M. Charles,[16] Ph. Charpentier,[49]
E. Chatzianagnostou,[38] M. Chefdeville,[10] C. Chen,[13] S. Chen,[5] Z. Chen,[7] A. Chernov,[41] S. Chernyshenko,[53]
X. Chiotopoulos,[79] V. Chobanova,[81] M. Chrzaszcz,[41] A. Chubykin,[44] V. Chulikov,[28] P. Ciambrone,[28]
X. Cid Vidal,[47] G. Ciezarek,[49] P. Cifra,[49] P. E. L. Clarke,[59] M. Clemencic,[49] H. V. Cliff,[56] J. Closier,[49]
C. Cocha Toapaxi,[22] V. Coco,[49] J. Cogan,[13] E. Cogneras,[11] L. Cojocariu,[43] S. Collaviti,[50] P. Collins,[49]
T. Colombo,[49] M. Colonna,[19] A. Comerma-Montells,[46] L. Congedo,[24] A. Contu,[32] N. Cooke,[60] I. Corredoira,[47]
A. Correia,[16] G. Corti,[49] J. Cottee Meldrum,[55] B. Couturier,[49] D. C. Craik,[51] M. Cruz Torres,[2,l]
E. Curras Rivera,[50] R. Currie,[59] C. L. Da Silva,[68] S. Dadabaev,[44] L. Dai,[71] X. Dai,[4] E. Dall'Occo,[49]
J. Dalseno,[47] C. D'Ambrosio,[49] J. Daniel,[11] A. Danilina,[44] P. d'Argent,[24] G. Darze,[3] A. Davidson,[57]
J. E. Davies,[63] A. Davis,[63] O. De Aguiar Francisco,[63] C. De Angelis,[32,m] F. De Benedetti,[49] J. de Boer,[38]
K. De Bruyn,[78] S. De Capua,[63] M. De Cian,[22] U. De Freitas Carneiro Da Graca,[2,n] E. De Lucia,[28]
J. M. De Miranda,[2] L. De Paula,[3] M. De Serio,[24,o] P. De Simone,[28] F. De Vellis,[19] J. A. de Vries,[79]
F. Debernardis,[24] D. Decamp,[10] V. Dedu,[13] S. Dekkers,[1] L. Del Buono,[16] B. Delaney,[65] H.-P. Dembinski,[19]
J. Deng,[8] V. Denysenko,[51] O. Deschamps,[11] F. Dettori,[32,m] B. Dey,[77] P. Di Nezza,[28] I. Diachkov,[44]
S. Didenko,[44] S. Ding,[69] L. Dittmann,[22] V. Dobishuk,[53] A. D. Docheva,[60] C. Dong,[4,p] A. M. Donohoe,[23]
F. Dordei,[32] A. C. dos Reis,[2] A. D. Dowling,[69] W. Duan,[72] P. Duda,[80] M. W. Dudek,[41] L. Dufour,[49] V. Duk,[34]
P. Durante,[49] M. M. Duras,[80] J. M. Durham,[68] O. D. Durmus,[77] A. Dziurda,[41] A. Dzyuba,[44] S. Easo,[58]
E. Eckstein,[18] U. Egede,[1] A. Egorychev,[44] V. Egorychev,[44] S. Eisenhardt,[59] E. Ejopu,[63] L. Eklund,[82]
M. Elashri,[66] J. Ellbracht,[19] S. Ely,[62] A. Ene,[43] J. Eschle,[69] S. Esen,[22] T. Evans,[63] F. Fabiano,[32,m]
L. N. Falcao,[2] Y. Fan,[7] B. Fang,[7] L. Fantini,[34,49,q] M. Faria,[50] K. Farmer,[59] D. Fazzini,[31,c] L. Felkowski,[80]
M. Feng,[5,7] M. Feo,[19] A. Fernandez Casani,[48] M. Fernandez Gomez,[47] A. D. Fernez,[67] F. Ferrari,[25,i]
F. Ferreira Rodrigues,[3] M. Ferrillo,[51] M. Ferro-Luzzi,[49] S. Filippov,[44] R. A. Fini,[24] M. Fiorini,[26,f] M. Firlej,[40]
K. L. Fischer,[64] D. S. Fitzgerald,[83] C. Fitzpatrick,[63] T. Fiutowski,[40] F. Fleuret,[15] M. Fontana,[25] L. F. Foreman,[63]
R. Forty,[49] D. Foulds-Holt,[56] V. Franco Lima,[3] M. Franco Sevilla,[67] M. Frank,[49] E. Franzoso,[26,f] G. Frau,[63]
C. Frei,[49] D. A. Friday,[63] J. Fu,[7] Q. Führing,[19,56,b] Y. Fujii,[1] T. Fulghesu,[16] E. Gabriel,[38] G. Galati,[24]
M. D. Galati,[38] A. Gallas Torreira,[47] D. Galli,[25,i] S. Gambetta,[59] M. Gandelman,[3] P. Gandini,[30] B. Ganie,[63]
H. Gao,[7] R. Gao,[64] T. Q. Gao,[56] Y. Gao,[8] Y. Gao,[6] Y. Gao,[8] L. M. Garcia Martin,[50] P. Garcia Moreno,[46]
J. García Pardiñas,[49] P. Gardner,[67] K. G. Garg,[8] L. Garrido,[46] C. Gaspar,[49] L. L. Gerken,[19] E. Gersabeck,[63]
M. Gersabeck,[20] T. Gershon,[57] S. Ghizzo,[29,j] Z. Ghorbanimoghaddam,[55] L. Giambastiani,[33,g] F. I. Giasemis,[16,r]
V. Gibson,[56] H. K. Giemza,[42] A. L. Gilman,[64] M. Giovannetti,[28] A. Gioventù,[46] L. Girardey,[63] C. Giugliano,[26,f]
M. A. Giza,[41] E. L. Gkougkousis,[62] F. C. Glaser,[14,22] V. V. Gligorov,[16,49] C. Göbel,[70] E. Golobardes,[45]
D. Golubkov,[44] A. Golutvin,[62,49,44] S. Gomez Fernandez,[46] W. Gomulka,[40] F. Goncalves Abrantes,[64] M. Goncerz,[41]

G. Gong,[4,p] J. A. Gooding,[19] I. V. Gorelov,[44] C. Gotti,[31] E. Govorkova,[65] J. P. Grabowski,[18]
L. A. Granado Cardoso,[49] E. Graugés,[46] E. Graverini,[50,s] L. Grazette,[57] G. Graziani, A. T. Grecu,[43]
L. M. Greeven,[38] N. A. Grieser,[66] L. Grillo,[60] S. Gromov,[44] C. Gu,[15] M. Guarise,[26] L. Guerry,[11] V. Guliaeva,[44]
P. A. Günther,[22] A.-K. Guseinov,[50] E. Gushchin,[44] Y. Guz,[6,49,44] T. Gys,[49] K. Habermann,[18] T. Hadavizadeh,[1]
C. Hadjivasiliou,[67] G. Haefeli,[50] C. Haen,[49] G. Hallett,[57] M. M. Halvorsen,[49] P. M. Hamilton,[67] J. Hammerich,[61]
Q. Han,[8] X. Han,[22,49] S. Hansmann-Menzemer,[22] L. Hao,[7] N. Harnew,[64] T. H. Harris,[1] M. Hartmann,[14]
S. Hashmi,[40] J. He,[7,t] F. Hemmer,[49] C. Henderson,[66] R. D. L. Henderson,[1,57] A. M. Hennequin,[49]
K. Hennessy,[61] L. Henry,[50] J. Herd,[62] P. Herrero Gascon,[22] J. Heuel,[17] A. Hicheur,[3] G. Hijano Mendizabal,[51]
J. Horswill,[63] R. Hou,[8] Y. Hou,[11] N. Howarth,[61] J. Hu,[72] W. Hu,[6] X. Hu,[4,p] W. Huang,[7] W. Hulsbergen,[38]
R. J. Hunter,[57] M. Hushchyn,[44] D. Hutchcroft,[61] M. Idzik,[40] D. Ilin,[44] P. Ilten,[66] A. Inglessi,[44] A. Iniukhin,[44]
A. Ishteev,[44] K. Ivshin,[44] R. Jacobsson,[49] H. Jage,[17] S. J. Jaimes Elles,[75,49,48] S. Jakobsen,[49] E. Jans,[38]
B. K. Jashal,[48] A. Jawahery,[67] V. Jevtic,[19,b] E. Jiang,[67] X. Jiang,[5,7] Y. Jiang,[7] Y. J. Jiang,[6] M. John,[64]
A. John Rubesh Rajan,[23] D. Johnson,[54] C. R. Jones,[56] T. P. Jones,[57] S. Joshi,[42] B. Jost,[49] J. Juan Castella,[56]
N. Jurik,[49] I. Juszczak,[41] D. Kaminaris,[50] S. Kandybei,[52] M. Kane,[59] Y. Kang,[4,p] C. Kar,[11] M. Karacson,[49]
D. Karpenkov,[44] A. Kauniskangas,[50] J. W. Kautz,[66] M. K. Kazanecki,[41] F. Keizer,[49] M. Kenzie,[56] T. Ketel,[38]
B. Khanji,[69] A. Kharisova,[44] S. Kholodenko,[35,49] G. Khreich,[14] T. Kirn,[17] V. S. Kirsebom,[31,c] O. Kitouni,[65]
S. Klaver,[39] N. Kleijne,[35,e] K. Klimaszewski,[42] M. R. Kmiec,[42] S. Koliiev,[53] L. Kolk,[19] A. Konoplyannikov,[44]
P. Kopciewicz,[49] P. Koppenburg,[38] M. Korolev,[44] I. Kostiuk,[38] O. Kot,[53] S. Kotriakhova, A. Kozachuk,[44]
P. Kravchenko,[44] L. Kravchuk,[44] M. Kreps,[57] P. Krokovny,[44] W. Krupa,[69] W. Krzemien,[42] O. Kshyvanskyi,[53]
S. Kubis,[80] M. Kucharczyk,[41] V. Kudryavtsev,[44] E. Kulikova,[44] A. Kupsc,[82] B. K. Kutsenko,[13] D. Lacarrere,[49]
P. Laguarta Gonzalez,[46] A. Lai,[32] A. Lampis,[32] D. Lancierini,[56] C. Landesa Gomez,[47] J. J. Lane,[1] R. Lane,[55]
G. Lanfranchi,[28] C. Langenbruch,[22] J. Langer,[19] O. Lantwin,[44] T. Latham,[57] F. Lazzari,[35,49,s] C. Lazzeroni,[54]
R. Le Gac,[13] H. Lee,[61] R. Lefèvre,[11] A. Leflat,[44] S. Legotin,[44] M. Lehuraux,[57] E. Lemos Cid,[49] O. Leroy,[13]
T. Lesiak,[41] E. D. Lesser,[49] B. Leverington,[22] A. Li,[4,p] C. Li,[13] H. Li,[72] K. Li,[8] L. Li,[63] M. Li,[8] P. Li,[7]
P.-R. Li,[73] Q. Li,[5,7] S. Li,[8] T. Li,[5,u] T. Li,[72] Y. Li,[8] Y. Li,[5] Z. Lian,[4,p] X. Liang,[69] S. Libralon,[48] C. Lin,[7]
T. Lin,[58] R. Lindner,[49] H. Linton,[62] V. Lisovskyi,[50] R. Litvinov,[32,49] F. L. Liu,[1] G. Liu,[72] K. Liu,[73] S. Liu,[5,7]
W. Liu,[8] Y. Liu,[59] Y. Liu,[73] Y. L. Liu,[62] G. Loachamin Ordonez,[70] A. Lobo Salvia,[46] A. Loi,[32] T. Long,[56]
J. H. Lopes,[3] A. Lopez Huertas,[46] S. López Soliño,[47] Q. Lu,[15] C. Lucarelli,[27] D. Lucchesi,[33,g]
M. Lucio Martinez,[79] V. Lukashenko,[38,53] Y. Luo,[6] A. Lupato,[33,v] E. Luppi,[26,f] K. Lynch,[23] X.-R. Lyu,[7]
G. M. Ma,[4,p] S. Maccolini,[19] F. Machefert,[14] F. Maciuc,[43] B. Mack,[69] I. Mackay,[64] L. M. Mackey,[69]
L. R. Madhan Mohan,[56] M. J. Madurai,[54] A. Maevskiy,[44] D. Magdalinski,[38] D. Maisuzenko,[44] M. W. Majewski,[40]
J. J. Malczewski,[41] S. Malde,[64] L. Malentacca,[49] A. Malinin,[44] T. Maltsev,[44] G. Manca,[32,m] G. Mancinelli,[13]
C. Mancuso,[30,14,k] R. Manera Escalero,[46] F. M. Manganella,[37] D. Manuzzi,[25] D. Marangotto,[30,k]
J. F. Marchand,[10] R. Marchevski,[50] U. Marconi,[25] E. Mariani,[16] S. Mariani,[49] C. Marin Benito,[46,49] J. Marks,[22]
A. M. Marshall,[55] L. Martel,[64] G. Martelli,[34,q] G. Martellotti,[36] L. Martinazzoli,[49] M. Martinelli,[31,c]
D. Martinez Gomez,[78] D. Martinez Santos,[81] F. Martinez Vidal,[48] A. Martorell i Granollers,[45] A. Massafferri,[2]
R. Matev,[49] A. Mathad,[49] V. Matiunin,[44] C. Matteuzzi,[69] K. R. Mattioli,[15] A. Mauri,[62] E. Maurice,[15]
J. Mauricio,[46] P. Mayencourt,[50] J. Mazorra de Cos,[48] M. Mazurek,[42] M. McCann,[62] L. Mcconnell,[23]
T. H. McGrath,[63] N. T. McHugh,[60] A. McNab,[63] R. McNulty,[23] B. Meadows,[66] G. Meier,[19] D. Melnychuk,[42]
F. M. Meng,[4,p] M. Merk,[38,79] A. Merli,[50] L. Meyer Garcia,[67] D. Miao,[5,7] H. Miao,[7] M. Mikhasenko,[76]
D. A. Milanes,[75,w] A. Minotti,[31,c] E. Minucci,[28] T. Miralles,[11] B. Mitreska,[19] D. S. Mitzel,[19] A. Modak,[58]
R. A. Mohammed,[64] R. D. Moise,[17] S. Mokhnenko,[44] E. F. Molina Cardenas,[83] T. Mombächer,[49] M. Monk,[57,1]
S. Monteil,[11] A. Morcillo Gomez,[47] G. Morello,[28] M. J. Morello,[35,e] M. P. Morgenthaler,[22] J. Moron,[40]
W. Morren,[38] A. B. Morris,[49] A. G. Morris,[13] R. Mountain,[69] H. Mu,[4,p] Z. M. Mu,[6] E. Muhammad,[57]
F. Muheim,[59] M. Mulder,[78] K. Müller,[51] F. Muñoz-Rojas,[9] R. Murta,[62] P. Naik,[61] T. Nakada,[50]
R. Nandakumar,[58] T. Nanut,[49] I. Nasteva,[3] M. Needham,[59] N. Neri,[30,k] S. Neubert,[18] N. Neufeld,[49]
P. Neustroev,[44] J. Nicolini,[19,14] D. Nicotra,[79] E. M. Niel,[49] N. Nikitin,[44] Q. Niu,[73] P. Nogarolli,[3] P. Nogga,[18]
C. Normand,[55] J. Novoa Fernandez,[47] G. Nowak,[66] C. Nunez,[83] H. N. Nur,[60] A. Oblakowska-Mucha,[40]
V. Obraztsov,[44] T. Oeser,[17] S. Okamura,[26,f] A. Okhotnikov,[44] O. Okhrimenko,[53] R. Oldeman,[32,m] F. Oliva,[59]

M. Olocco,[19] C. J. G. Onderwater,[79] R. H. O’Neil,[49] D. Osthues,[19] J. M. Otalora Goicochea,[3] P. Owen,[51]
A. Oyanguren,[48] O. Ozcelik,[59] F. Paciolla,[35,x] A. Padee,[42] K. O. Padeken,[18] B. Pagare,[57] P. R. Pais,[22]
T. Pajero,[49] A. Palano,[24,†] M. Palutan,[28] X. Pan,[4,p] G. Panshin,[44] L. Paolucci,[57] A. Papanestis,[58,49]
M. Pappagallo,[24,o] L. L. Pappalardo,[26,f] C. Pappenheimer,[66] C. Parkes,[63] D. Parmar,[76] B. Passalacqua,[26,f]
G. Passaleva,[27] D. Passaro,[35,49,e] A. Pastore,[24] M. Patel,[62] J. Patoc,[64] C. Patrignani,[25,i] A. Paul,[69]
C. J. Pawley,[79] A. Pellegrino,[38] J. Peng,[5,7] M. Pepe Altarelli,[28] S. Perazzini,[25] D. Pereima,[44]
H. Pereira Da Costa,[68] A. Pereiro Castro,[47] P. Perret,[11] A. Perrevoort,[78] A. Perro,[49,13] M. J. Peters,[66] K. Petridis,[55]
A. Petrolini,[29,j] J. P. Pfaller,[66] H. Pham,[69] L. Pica,[35,e] M. Piccini,[34] L. Piccolo,[32] B. Pietrzyk,[10] G. Pietrzyk,[14]
R. N. Pilato,[61] D. Pinci,[36] F. Pisani,[49] M. Pizzichemi,[31,49,c] V. Placinta,[43] M. Plo Casasus,[47] T. Poeschl,[49]
F. Polci,[16] M. Poli Lener,[28] A. Poluektov,[13] N. Polukhina,[44] I. Polyakov,[44] E. Polycarpo,[3] S. Ponce,[49]
D. Popov,[7] S. Poslavskii,[44] K. Prasanth,[59] C. Prouve,[81] D. Provenzano,[32,m] V. Pugatch,[53] G. Punzi,[35,s]
S. Qasim,[51] Q. Q. Qian,[6] W. Qian,[7] N. Qin,[4,p] S. Qu,[4,p] R. Quagliani,[49] R. I. Rabadan Trejo,[57]
J. H. Rademacker,[55] M. Rama,[35] M. Ramírez García,[83] V. Ramos De Oliveira,[70] M. Ramos Pernas,[57]
M. S. Rangel,[3] F. Ratnikov,[44] G. Raven,[39] M. Rebollo De Miguel,[48] F. Redi,[30,v] J. Reich,[55] F. Reiss,[63] Z. Ren,[7]
P. K. Resmi,[64] R. Ribatti,[50] G. R. Ricart,[15,12] D. Riccardi,[35,e] S. Ricciardi,[58] K. Richardson,[65]
M. Richardson-Slipper,[59] K. Rinnert,[61] P. Robbe,[14,49] G. Robertson,[60] E. Rodrigues,[61] A. Rodriguez Alvarez,[46]
E. Rodriguez Fernandez,[47] J. A. Rodriguez Lopez,[75] E. Rodriguez Rodriguez,[47] J. Roensch,[19] A. Rogachev,[44]
A. Rogovskiy,[58] D. L. Rolf,[49] P. Roloff,[49] V. Romanovskiy,[66] A. Romero Vidal,[47] G. Romolini,[26]
F. Ronchetti,[50] T. Rong,[6] M. Rotondo,[28] S. R. Roy,[22] M. S. Rudolph,[69] M. Ruiz Diaz,[22] R. A. Ruiz Fernandez,[47]
J. Ruiz Vidal,[82,y] A. Ryzhikov,[44] J. Ryzka,[40] J. J. Saavedra-Arias,[9] J. J. Saborido Silva,[47] R. Sadek,[15]
N. Sagidova,[44] D. Sahoo,[77] N. Sahoo,[54] B. Saitta,[32,m] M. Salomoni,[31,49,c] I. Sanderswood,[48] R. Santacesaria,[36]
C. Santamarina Rios,[47] M. Santimaria,[28,49] L. Santoro,[2] E. Santovetti,[37] A. Saputi,[26,49] D. Saranin,[44]
A. Sarnatskiy,[78] G. Sarpis,[59] M. Sarpis,[63] C. Satriano,[36,z] A. Satta,[37] M. Saur,[6] D. Savrina,[44] H. Sazak,[17]
F. Sborzacchi,[49,28] L. G. Scantlebury Smead,[64] A. Scarabotto,[19] S. Schael,[17] S. Scherl,[61] M. Schiller,[60]
H. Schindler,[49] M. Schmelling,[21] B. Schmidt,[49] S. Schmitt,[17] H. Schmitz,[18] O. Schneider,[50] A. Schopper,[49]
N. Schulte,[19] S. Schulte,[50] M. H. Schune,[14] R. Schwemmer,[49] G. Schwering,[17] B. Sciascia,[28] A. Sciuccati,[49]
I. Segal,[76] S. Sellam,[47] A. Semennikov,[44] T. Senger,[51] M. Senghi Soares,[39] A. Sergi,[29,j] N. Serra,[51]
L. Sestini,[33] A. Seuthe,[19] Y. Shang,[6] D. M. Shangase,[83] M. Shapkin,[44] R. S. Sharma,[69] I. Shchemerov,[44]
L. Shchutska,[50] T. Shears,[61] L. Shekhtman,[44] Z. Shen,[6] S. Sheng,[5,7] V. Shevchenko,[44] B. Shi,[7] Q. Shi,[7]
Y. Shimizu,[14] E. Shmanin,[25] R. Shorkin,[44] J. D. Shupperd,[69] R. Silva Coutinho,[69] G. Simi,[33,g] S. Simone,[24,o]
N. Skidmore,[57] T. Skwarnicki,[69] M. W. Slater,[54] J. C. Smallwood,[64] E. Smith,[65] K. Smith,[68] M. Smith,[62]
A. Snoch,[38] L. Soares Lavra,[59] M. D. Sokoloff,[66] F. J. P. Soler,[60] A. Solomin,[44,55] A. Solovev,[44] I. Solovyev,[44]
N. S. Sommerfeld,[18] R. Song,[1] Y. Song,[50] Y. Song,[4,p] Y. S. Song,[6] F. L. Souza De Almeida,[69]
B. Souza De Paula,[3] E. Spadaro Norella,[29,j] E. Spedicato,[25] J. G. Speer,[19] E. Spiridenkov,[44] P. Spradlin,[60]
V. Sriskaran,[49] F. Stagni,[49] M. Stahl,[76] S. Stahl,[49] S. Stanislaus,[64] M. Stefaniak,[84] E. N. Stein,[49]
O. Steinkamp,[51] O. Stenyakin,[44] H. Stevens,[19] D. Strekalina,[44] Y. Su,[7] F. Suljik,[64] J. Sun,[32] L. Sun,[74]
D. Sundfeld,[2] W. Sutcliffe,[51] P. N. Swallow,[54] K. Swientek,[40] F. Swystun,[56] A. Szabelski,[42] T. Szumlak,[40]
Y. Tan,[4,p] Y. Tang,[74] M. D. Tat,[22] A. Terentev,[44] F. Terzuoli,[35,49,x] F. Teubert,[49] E. Thomas,[49]
D. J. D. Thompson,[54] H. Tilquin,[62] V. Tisserand,[11] S. T’Jampens,[10] M. Tobin,[5,49] L. Tomassetti,[26,f]
G. Tonani,[30,k] X. Tong,[6] T. Tork,[30] D. Torres Machado,[2] L. Toscano,[19] D. Y. Tou,[4,p] C. Trippl,[45] G. Tuci,[22]
N. Tuning,[38] L. H. Uecker,[22] A. Ukleja,[40] D. J. Unverzagt,[22] B. Urbach,[59] A. Usachov,[39] A. Ustyuzhanin,[44]
U. Uwer,[22] V. Vagnoni,[25] V. Valcarce Cadenas,[47] G. Valenti,[25] N. Valls Canudas,[49] J. van Eldik,[49]
H. Van Hecke,[68] E. van Herwijnen,[62] C. B. Van Hulse,[47,aa] R. Van Laak,[50] M. van Veghel,[38] G. Vasquez,[51]
R. Vazquez Gomez,[46] P. Vazquez Regueiro,[47] C. Vázquez Sierra,[47] S. Vecchi,[26] J. J. Velthuis,[55] M. Veltri,[27,bb]
A. Venkateswaran,[50] M. Verdoglia,[32] M. Vesterinen,[57] D. Vico Benet,[64] P. Vidrier Villalba,[46] M. Vieites Diaz,[47]
X. Vilasis-Cardona,[45] E. Vilella Figueras,[61] A. Villa,[25] P. Vincent,[16] F. C. Volle,[54] D. vom Bruch,[13]
N. Voropaev,[44] K. Vos,[79] C. Vrahas,[59] J. Wagner,[19] J. Walsh,[35] E. J. Walton,[1,57] G. Wan,[6] C. Wang,[22]
G. Wang,[8] H. Wang,[73] J. Wang,[6] J. Wang,[5] J. Wang,[4,p] J. Wang,[74] M. Wang,[30] N. W. Wang,[7] R. Wang,[55]
X. Wang,[8] X. Wang,[72] X. W. Wang,[62] Y. Wang,[6] Y. W. Wang,[73] Z. Wang,[14] Z. Wang,[4,p] Z. Wang,[30]

J. A. Ward,[57,1] M. Waterlaat,[49] N. K. Watson,[54] D. Websdale,[62] Y. Wei,[6] J. Wendel,[81] B. D. C. Westhenry,[55]
C. White,[56] M. Whitehead,[60] E. Whiter,[54] A. R. Wiederhold,[63] D. Wiedner,[19] G. Wilkinson,[64]
M. K. Wilkinson,[66] M. Williams,[65] M. J. Williams,[49] M. R. J. Williams,[59] R. Williams,[56] Z. Williams,[55]
F. F. Wilson,[58] M. Winn,[12] W. Wislicki,[42] M. Witek,[41] L. Witola,[22] G. Wormser,[14] S. A. Wotton,[56] H. Wu,[69]
J. Wu,[8] X. Wu,[74] Y. Wu,[6] Z. Wu,[7] K. Wyllie,[49] S. Xian,[72] Z. Xiang,[5] Y. Xie,[8] T. X. Xing,[30] A. Xu,[35]
L. Xu,[4,p] L. Xu,[4,p] M. Xu,[57] Z. Xu,[49] Z. Xu,[7] Z. Xu,[5] K. Yang,[62] S. Yang,[7] X. Yang,[6] Y. Yang,[29,j]
Z. Yang,[6] V. Yeroshenko,[14] H. Yeung,[63] H. Yin,[8] X. Yin,[7] C. Y. Yu,[6] J. Yu,[71] X. Yuan,[5] Y Yuan,[5,7]
E. Zaffaroni,[50] M. Zavertyaev,[21] M. Zdybal,[41] F. Zenesini,[25] C. Zeng,[5,7] M. Zeng,[4,p] C. Zhang,[6] D. Zhang,[8]
J. Zhang,[7] L. Zhang,[4,p] S. Zhang,[71] S. Zhang,[64] Y. Zhang,[6] Y. Z. Zhang,[4,p] Z. Zhang,[4,p] Y. Zhao,[22]
A. Zhelezov,[22] S. Z. Zheng,[6] X. Z. Zheng,[4,p] Y. Zheng,[7] T. Zhou,[6] X. Zhou,[8] Y. Zhou,[7] V. Zhovkovska,[57]
L. Z. Zhu,[7] X. Zhu,[4,p] X. Zhu,[8] V. Zhukov,[17] J. Zhuo,[48] Q. Zou,[5,7] D. Zuliani,[33,g] and G. Zunica[50]

(LHCb Collaboration)

[1] *School of Physics and Astronomy, Monash University, Melbourne, Australia*
[2] *Centro Brasileiro de Pesquisas Físicas (CBPF), Rio de Janeiro, Brazil*
[3] *Universidade Federal do Rio de Janeiro (UFRJ), Rio de Janeiro, Brazil*
[4] *Department of Engineering Physics, Tsinghua University, Beijing, China*
[5] *Institute of High Energy Physics (IHEP), Beijing, China*
[6] *School of Physics State Key Laboratory of Nuclear Physics and Technology, Peking University, Beijing, China*
[7] *University of Chinese Academy of Sciences, Beijing, China*
[8] *Institute of Particle Physics, Central China Normal University, Wuhan, Hubei, China*
[9] *Consejo Nacional de Rectores (CONARE), San Jose, Costa Rica*
[10] *Université Savoie Mont Blanc, CNRS, IN2P3-LAPP, Annecy, France*
[11] *Université Clermont Auvergne, CNRS/IN2P3, LPC, Clermont-Ferrand, France*
[12] *Université Paris-Saclay, Centre d'Etudes de Saclay (CEA), IRFU, Saclay, France, Gif-Sur-Yvette, France*
[13] *Aix Marseille Univ, CNRS/IN2P3, CPPM, Marseille, France*
[14] *Université Paris-Saclay, CNRS/IN2P3, IJCLab, Orsay, France*
[15] *Laboratoire Leprince-Ringuet, CNRS/IN2P3, Ecole Polytechnique, Institut Polytechnique de Paris, Palaiseau, France*
[16] *LPNHE, Sorbonne Université, Paris Diderot Sorbonne Paris Cité, CNRS/IN2P3, Paris, France*
[17] *I. Physikalisches Institut, RWTH Aachen University, Aachen, Germany*
[18] *Universität Bonn—Helmholtz-Institut für Strahlen und Kernphysik, Bonn, Germany*
[19] *Fakultät Physik, Technische Universität Dortmund, Dortmund, Germany*
[20] *Physikalisches Institut, Albert-Ludwigs-Universität Freiburg, Freiburg, Germany*
[21] *Max-Planck-Institut für Kernphysik (MPIK), Heidelberg, Germany*
[22] *Physikalisches Institut, Ruprecht-Karls-Universität Heidelberg, Heidelberg, Germany*
[23] *School of Physics, University College Dublin, Dublin, Ireland*
[24] *INFN Sezione di Bari*, Bari, Italy
[25] *INFN Sezione di Bologna, Bologna, Italy*
[26] *INFN Sezione di Ferrara, Ferrara, Italy*
[27] *INFN Sezione di Firenze, Firenze, Italy*
[28] *INFN Laboratori Nazionali di Frascati, Frascati, Italy*
[29] *INFN Sezione di Genova, Genova, Italy*
[30] *INFN Sezione di Milano, Milano, Italy*
[31] *INFN Sezione di Milano-Bicocca, Milano, Italy*
[32] *INFN Sezione di Cagliari, Monserrato, Italy*
[33] *INFN Sezione di Padova, Padova, Italy*
[34] *INFN Sezione di Perugia, Perugia, Italy*
[35] *INFN Sezione di Pisa, Pisa, Italy*
[36] *INFN Sezione di Roma La Sapienza, Roma, Italy*
[37] *INFN Sezione di Roma Tor Vergata, Roma, Italy*
[38] *Nikhef National Institute for Subatomic Physics, Amsterdam, Netherlands*
[39] *Nikhef National Institute for Subatomic Physics and VU University Amsterdam, Amsterdam, Netherlands*
[40] *AGH—University of Krakow, Faculty of Physics and Applied Computer Science, Kraków, Poland*

[41]Henryk Niewodniczanski Institute of Nuclear Physics Polish Academy of Sciences, Kraków, Poland
[42]National Center for Nuclear Research (NCBJ), Warsaw, Poland
[43]Horia Hulubei National Institute of Physics and Nuclear Engineering, Bucharest-Magurele, Romania
[44]Authors affiliated with an institute formerly covered by a cooperation agreement with CERN
[45]DS4DS, La Salle, Universitat Ramon Llull, Barcelona, Spain
[46]ICCUB, Universitat de Barcelona, Barcelona, Spain
[47]Instituto Galego de Física de Altas Enerxías (IGFAE), Universidade de Santiago de Compostela, Santiago de Compostela, Spain
[48]Instituto de Fisica Corpuscular, Centro Mixto Universidad de Valencia—CSIC, Valencia, Spain
[49]European Organization for Nuclear Research (CERN), Geneva, Switzerland
[50]Institute of Physics, Ecole Polytechnique Fédérale de Lausanne (EPFL), Lausanne, Switzerland
[51]Physik-Institut, Universität Zürich, Zürich, Switzerland
[52]NSC Kharkiv Institute of Physics and Technology (NSC KIPT), Kharkiv, Ukraine
[53]Institute for Nuclear Research of the National Academy of Sciences (KINR), Kyiv, Ukraine
[54]School of Physics and Astronomy, University of Birmingham, Birmingham, United Kingdom
[55]H.H. Wills Physics Laboratory, University of Bristol, Bristol, United Kingdom
[56]Cavendish Laboratory, University of Cambridge, Cambridge, United Kingdom
[57]Department of Physics, University of Warwick, Coventry, United Kingdom
[58]STFC Rutherford Appleton Laboratory, Didcot, United Kingdom
[59]School of Physics and Astronomy, University of Edinburgh, Edinburgh, United Kingdom
[60]School of Physics and Astronomy, University of Glasgow, Glasgow, United Kingdom
[61]Oliver Lodge Laboratory, University of Liverpool, Liverpool, United Kingdom
[62]Imperial College London, London, United Kingdom
[63]Department of Physics and Astronomy, University of Manchester, Manchester, United Kingdom
[64]Department of Physics, University of Oxford, Oxford, United Kingdom
[65]Massachusetts Institute of Technology, Cambridge, Massachusetts, USA
[66]University of Cincinnati, Cincinnati, Ohio, USA
[67]University of Maryland, College Park, Maryland, USA
[68]Los Alamos National Laboratory (LANL), Los Alamos, New Mexico, USA
[69]Syracuse University, Syracuse, New York, USA
[70]Pontifícia Universidade Católica do Rio de Janeiro (PUC-Rio), Rio de Janeiro, Brazil (associated with Universidade Federal do Rio de Janeiro (UFRJ), Rio de Janeiro, Brazil)
[71]School of Physics and Electronics, Hunan University, Changsha City, China (associated with Institute of Particle Physics, Central China Normal University, Wuhan, Hubei, China)
[72]Guangdong Provincial Key Laboratory of Nuclear Science, Guangdong-Hong Kong Joint Laboratory of Quantum Matter, Institute of Quantum Matter, South China Normal University, Guangzhou, China (associated with Department of Engineering Physics, Tsinghua University, Beijing, China)
[73]Lanzhou University, Lanzhou, China (associated with Institute of High Energy Physics (IHEP), Beijing, China)
[74]School of Physics and Technology, Wuhan University, Wuhan, China (associated with Department of Engineering Physics, Tsinghua University, Beijing, China)
[75]Departamento de Fisica, Universidad Nacional de Colombia, Bogota, Colombia (associated with LPNHE, Sorbonne Université, Paris Diderot Sorbonne Paris Cité, CNRS/IN2P3, Paris, France)
[76]Ruhr Universitaet Bochum, Fakultaet für Physik und Astronomie, Bochum, Germany (associated with Fakultät Physik, Technische Universität Dortmund, Dortmund, Germany)
[77]Eotvos Lorand University, Budapest, Hungary (associated with European Organization for Nuclear Research (CERN), Geneva, Switzerland)
[78]Van Swinderen Institute, University of Groningen, Groningen, Netherlands (associated with Nikhef National Institute for Subatomic Physics, Amsterdam, Netherlands)
[79]Universiteit Maastricht, Maastricht, Netherlands (associated with Nikhef National Institute for Subatomic Physics, Amsterdam, Netherlands)
[80]Tadeusz Kosciuszko Cracow University of Technology, Cracow, Poland (associated with Henryk Niewodniczanski Institute of Nuclear Physics Polish Academy of Sciences, Kraków, Poland)

[81]*Universidade da Coruña, A Coruña, Spain*
(associated with DS4DS, La Salle, Universitat Ramon Llull, Barcelona, Spain)
[82]*Department of Physics and Astronomy, Uppsala University, Uppsala, Sweden*
(associated with School of Physics and Astronomy, University of Glasgow, Glasgow, United Kingdom)
[83]*University of Michigan, Ann Arbor, Michigan, USA*
(associated with Syracuse University, Syracuse, New York, USA)
[84]*Ohio State University, Columbus, United States*
(associated with Los Alamos National Laboratory (LANL), Los Alamos, New Mexico, USA)

[†] Contact author: antimo.palano@cern.ch.
[a] Deceased.
[b] Also at Lamarr Institute for Machine Learning and Artificial Intelligence, Dortmund, Germany.
[c] Also at Università degli Studi di Milano-Bicocca, Milano, Italy.
[d] Also at Università di Roma Tor Vergata, Roma, Italy.
[e] Also at Scuola Normale Superiore, Pisa, Italy.
[f] Also at Università di Ferrara, Ferrara, Italy.
[g] Also at Università di Padova, Padova, Italy.
[h] Also at Facultad de Ciencias Fisicas, Madrid, Spain.
[i] Also at Università di Bologna, Bologna, Italy.
[j] Also at Università di Genova, Genova, Italy.
[k] Also at Università degli Studi di Milano, Milano, Italy.
[l] Also at Universidad Nacional Autónoma de Honduras, Tegucigalpa, Honduras.
[m] Also at Università di Cagliari, Cagliari, Italy.
[n] Also at Centro Federal de Educacão Tecnológica Celso Suckow da Fonseca, Rio De Janeiro, Brazil.
[o] Also at Università di Bari, Bari, Italy.
[p] Also at Center for High Energy Physics, Tsinghua University, Beijing, China.
[q] Also at Università di Perugia, Perugia, Italy.
[r] Also at LIP6, Sorbonne Université, Paris, France.
[s] Also at Università di Pisa, Pisa, Italy.
[t] Also at Hangzhou Institute for Advanced Study, UCAS, Hangzhou, China.
[u] Also at School of Physics and Electronics, Henan University, Kaifeng, China.
[v] Also at Università di Bergamo, Bergamo, Italy.
[w] Also at Universidad de Ingeniería y Tecnología (UTEC), Lima, Peru.
[x] Also at Università di Siena, Siena, Italy.
[y] Also at Department of Physics/Division of Particle Physics, Lund, Sweden.
[z] Also at Università della Basilicata, Potenza, Italy.
[aa] Also at Universidad de Alcalá, Alcalá de Henares, Spain.
[bb] Also at Università di Urbino, Urbino, Italy.